


ORIGINAL RESEARCH

The digital twin of complex shipboard DC microgrids: The high-performing synergy of compiled models and HIL platform in the dynamics emulation of zonal power electronic power distribution systems

Andrea Alessia Tavagnutti | Andrea Vicenzutti | Massimiliano Chiandone |
Daniele Bosich  | Giorgio Sulligoi

Department of Engineering and Architecture,
University of Trieste, Trieste, Italy

Correspondence

Daniele Bosich, Department of Engineering and
Architecture, University of Trieste, Trieste, Italy.
Email: dbosich@units.it

© 2023 IEEE. Reprinted, with permission, from [D. Bosich, M. Chiandone, G. Sulligoi, A. A. Tavagnutti, A. Vicenzutti, “High-Performance Megawatt-Scale MVDC Zonal Electrical Distribution System Based on Power Electronics Open System Interfaces” IEEE Transactions on Transportation Electrification Vol.: 9, Issue: 3, 2023].

© 2022 IEEE. Reprinted, with permission, from [A. A. Tavagnutti, S. Bertagna, D. Bosich, V. Bucci and G. Sulligoi, “Open Source Hardware in the Loop Real-time Simulation of Zonal DC systems” Proc. 2022 Open Source Modelling and Simulation of Energy Systems (OSMSSES), 2022, pp. 1-6].

Funding information

European Union, Horizon Europe
Program—V-ACCESS Project, Grant/Award
Number: 101096831

Abstract

Nowadays, resilience is a crucial attribute to be pursued in advanced shipboard DC microgrids. When the power distribution is zonal, the presence of autonomous-controlled converters guarantees both power use and resiliency improvement. The adoption of bidirectional controlled devices ensures power routing among generating units, storage, and loads. Moreover, zonal electrical distribution systems are effective in applying the optimization algorithms for green, safe, and high-performing ship operation. In zonal DC microgrids, real-time cooperation among controlled converters through properly set communication protocols enables the ship mission achievement. To this aim, functional tests are to be done on such complex power infrastructure. The digital twin approach provides the de-risking step before the onboard deployment for controlled systems and communication. A zonal DC shipboard microgrid is the case study to test the synergy between compiled models and power converters on two hardware in the loop platforms, then verified by experiment in this paper. The first platform exploits the Linux real time application interface on the average value models of converters. This solution is then compared with a platform that utilizes the Typhoon hardware in the loop environment, proposing a combination of average value models and detailed switching models for the real-time emulation of controlled grid.

1 | INTRODUCTION

The climate change issue is pushing towards a revolution in the sources responsible for supplying the worldwide power systems. The increasing adoption of renewable sources can significantly reduce the carbon footprint, while also forcing a radical change in how controlled power grids are managed, their structure, and their required functions. The old paradigm of electromechanical-based power generation and passive networks is now shifting to a new power system paradigm based on interconnected microgrids and smart grids, distributed renewable power sources, and active networks. In such a context,

power-electronics constitutes the enabling technology, where power electronic power distribution systems [1] allow for innovative services and high dynamic performance to be delivered [2, 3]. Such an evolution towards “energy digitalization” not only ensures the exploitation of green sources and storage, but also enables flexibility and resilience as new powerful features on advanced controlled power grids. Maritime transportation is also involved in this all-encompassing scenario. Efficiency, environmental-friendliness, flexibility, and modularity are becoming the main drivers for designing onboard power systems [4]. Thus, innovative and high performing solutions are being proposed to meet these demands [5]. These new

This is an open access article under the terms of the [Creative Commons Attribution](https://creativecommons.org/licenses/by/4.0/) License, which permits use, distribution and reproduction in any medium, provided the original work is properly cited.

© 2025 The Author(s). *IET Power Electronics* published by John Wiley & Sons Ltd on behalf of The Institution of Engineering and Technology.

solutions integrate energy storage systems (ESS) to manage highly variable loads and provide support to the power system (either enabling zero emission navigation or allowing to optimize the operation of the onboard generators to lower their fuel consumption), and use advanced power management systems (PMSs) and energy management systems (EMSs) for introducing both flexibility and optimization to the conventional onboard operation framework [6, 7]. Upgradability is also a significant aspect for today maritime power systems, which are designed and built to last tens of years. In such a period, technological advancements may revolutionize the sector. Thus, enabling a certain amount of openness and applying a modular approach to the onboard power systems, makes them easier to maintain and ensure the possibility to upgrade them in the future with a lower effort in respect to conventional solutions.

The zonal electrical distribution systems (ZEDS), whose concept is discussed in the IEEE Std. 1826–2020 [8], are the emerging solution to this aim. The ZEDS are designed to be used in all the applications in which an advanced power system may be useful (e.g. data centres, hospitals, green steel plants), including ships. In fact, this architecture began to be discussed in the 90s, particularly in the maritime sector [9–11] for applications where increased survivability and reliability performance were critical. Today it has become a viable solution for all applications requiring the integration of different energy sources and loads is to be done, while guaranteeing the possibility of both interconnected and islanded operation and enabling high performance and reliability. Consequently, in 2012, the first revision of the IEEE Std. 1826 [8] was released, to provide a framework for the zonal interfaces' definition and design, building on previous standards and concepts [12–14]. A key element of modern ZEDS are the power electronics converters, which enable the strict control and coordinated management of all the electrical variables at the zonal boundaries, ensuring correct operation [3, 15]. Moreover, power electronics converters allow the integration of various power sources, ESS, and loads, with the desired flexibility and modularity. Although the ZEDS concept is not based on a specific power distribution, the presence of several conversion stages pairs well with the direct current (DC), allowing the reduction of converter stages, the removal of control loops (no frequency and phase to be managed), easing the Power Quality issues solution, and in general making the power system design and operation easier. To this aim and considering the amount of electrical power required by modern ships, the medium voltage DC (MVDC) was proposed as a distribution concept for All Electric Ships (AESs), where the final result is an MVDC ZEDS. The pioneer on such topic was the US Navy in the early 2000s [16, 17], while nowadays MVDC ZEDS are still to be a standardized and commercially available product. Some topics are still under investigation, for example voltage stability [18, 19], fault management, fault detection and protections coordination [20, 21] and PMSs [22]. The controlled DC grids on ships require the presence of various types of power electronic converters, whose action is managed/optimized by a central unit. Despite the diversity in switching interfaces, topology, or architecture, each of these converters has a set of control functions mostly

implemented as a software layer running on a CPU. In an interconnected power system, these devices are interfaced by power lines/buses and data infrastructure, while the operation is coordinated by central devices [23]. To develop these devices, which mix hardware and software elements, at both control and power levels, the most used methodology is the hardware-in-the-loop emulation (HIL). This approach helps in both design and validation phases [24]. Several applications can be implemented through detailed models to obtain the high-fidelity transients simulation required to develop fast control functions. However, it is not always necessary to apply such detailed models, where each electronic device switching can be appreciated and analysed in depth, whose complexity is undeniable. Although this feature is required for developers in power electronics converters and for some specific scopes (e.g. electromagnetic noise evaluation), system integrators can frequently rely on simpler models (for each component) that allow the development and de-risking of complex interconnected systems timely and with a less computational-intense approach. Among these simpler modelling approaches, average value models (AVM) are the easier to apply, while performing sufficiently close to detailed models for several of the system design needs (a comparison among AVM and detailed models is offered in [25]). In this example, the AVM approach results sufficient in testing the behaviour of an entire interconnected microgrid with a centralized controller. Another option is to combine the AVMs and the more detailed switching models in the same emulation environment, this makes it possible to exploit the advantages of both solutions. Although this approach can be found in literature for testing single power converters [26], the consequent development on multiple converters solution is not sufficiently developed, so it deserves additional attention. To this aim, in the present work the authors propose the integration of AVMs and switching models for studying a complete DC power grid with zonal architecture.

Regarding the above-mentioned software layer for implementing control functions, there has been an ever-increasing use of open-source software and architectures in recent years. This trend started from the application of open-source tools for performing power system analyses [27], but it is spreading to the development of control algorithms [28]. Following this trend, this paper presents two HIL implementations of a DC-based power electronics power distribution system. One is based on an open-source real time operating system (RTOS), while the other is built upon the Typhoon HIL hardware and software packages. Both implementations include the mathematical model of the electrical grid and the data network part of the system at level three of the ISO-OSI model (therefore with IP addresses, network protocols and interactions at the TCP and UDP levels). However, the physical levels are slightly different from the real system (i.e. in the HIL implementations there are fewer network cards and fewer switches). The implementation built with RTAI provides greater control over the communication network settings (individual IP address and protocol implementation can be freely adjusted) but cannot be used to simulate fast transients (such as power electronics' switching), while Typhoon HIL forces the use of preset protocols and

cards (thus being faster to implement, but less flexible for communication layer testing) but enables the simulation of faster dynamics (if required). In this regard, the RTAI [29] is adopted to implement the power system modelled through the AVM approach for real time simulation. Communications between all devices are carried over an IP-based data network, using standard application-level protocols. The paper goal is to validate the PMS operation, by connecting it to a model of the power distribution system (thus exploiting the HIL approach for control systems' de-risking). The PMS is implemented by a commercial programmable logic controller (PLC). The mathematical model of the grid obtained is simulated in real time and the communications between the various converters have been implemented at IP level exactly as in the real plant. Accuracy and cost-effectiveness of the solutions described are two of the major benefits of the proposed solution.

The AVM modelling used in the RTAI implementation is the baseline for the construction of an alternative digital twin implementation, that combines AVMs and more detailed switching models. The environment used to build such a digital twin is the Typhoon HIL one (however other similar environment could be also exploited). The present work is thus aimed at providing a multi-tools simulating methodology to basically reproduce two time-scale dynamics on controlled DC power grid. The designed platforms are then to be capable of simulating both very fast transients (i.e. power electronics switching), as well as correctly representing slow dynamics, like the multi-zone control system operation. By considering that a single model to perform all digital twin tasks at different layers is still not widely available for an entire DC zonal DC grid, this paper therefore presents and compares two tools for implementing a digital twin. The aim is to provide information useful for the selection of the correct tool for each de-risking step, and depending on the specific tests that need to be performed. The paper is organized as in the following. The Section 2 describes the case study power system, its control architecture, and the mathematical modelling applied to implement it into the two HIL systems analysed here. In Section 3, the specific implementations of the DC grid in the digital twins based on the two different

HIL approaches are described. The Section 4 is dedicated to present test results of both implementations, comparing them with experimental results. Section 5 concludes the paper.

2 | ZONAL DC POWER DISTRIBUTION FOR ADVANCED NAVAL VESSELS

The paper discusses a digital twin for an advanced DC power system based on zonal distribution. The case study is the MW-scale demonstrator that has been already presented in [30], where a MW test has been described starting from the basic knowledge on IEEE standards [8, 12, 13]. In the present context, the most important characteristics of the testbed are here recovered, while a detailed description of the digital twin is the main contribution. In the following subsections, the zonal distribution is addressed with the necessary information about control architecture and system modelling. In next sections, the main attention is put on the digital twins, the communication protocols, and the final test during the onsite experimental campaign. The last test will be essential to validate the digital twins and their capability in revealing the dynamic behaviour of the DC zonal microgrid.

2.1 | Zonal DC topology

The advanced distribution under study in Figure 1 is the natural implementation of what proposed in the IEEE Std. 1709 [31]. In this standard, the first idea of zonal DC grid was revealed in 2010. The considered DC power grid is powered by two main feeders (namely MVDC Bus1-Bus2) with a rated voltage of 1050 V. Such a value is sufficient to categorize such a system as medium voltage DC microgrid. In the left part of the central scheme, a busbar connector is aimed at closing the distribution, thus enabling parallel feeding. Two diesel generators (i.e. DG1-DG2) in the left half are responsible for powering the DC system, providing 2 and 1.5 MW respectively as rated powers. Regarding the DC system interfaces, the AC/DC

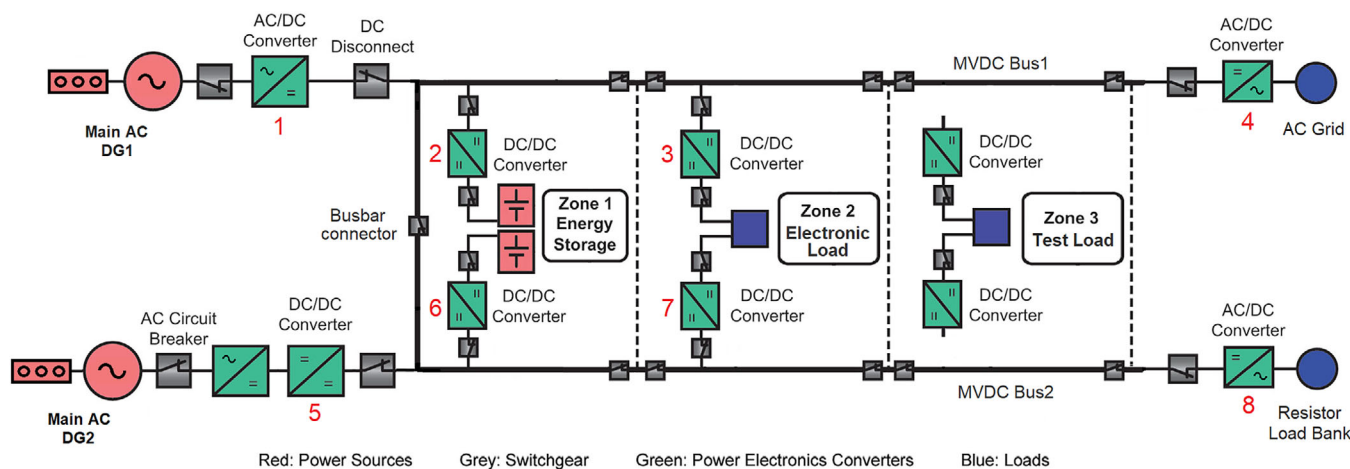


FIGURE 1 Zonal DC shipboard microgrid [30].

TABLE 1 Converters data.

Modules	Rated power [kW]	DC bus capacitance [mF]	Control mode
1 2	3360	24	Power
2 1	1680	12	Bus voltage
3 1	1680	12	Load voltage
4 2	3360	24	Power
5 1	1680	12	Power
6 1	1680	12	Bus voltage
7 1	1680	12	Load voltage
8 2	3360	24	Voltage and frequency

Converter 1 connects the DG1 to MVDC bus1, while the cascade of diode rectifier and DC/DC converter 5 is used to make the power input from DG2 genset available on MVDC Bus2. The loads are shown in the right part by blue circles. In this regard, the active front end AC/DC converter 4 ensures the bidirectional power flow from/to the external AC grid, whereas the AC/DC inverter 8 feeds the three-phase load resistors. Specifically, the connection to the factory AC grid is used to model the ship propulsion and the resistor bank represents onboard loads. Until now, the description has explored the elements outside the zonal arrangement. Moving to the middle of the scheme, the zonal distribution is developed in three adjacent zones. To increase overall system resiliency, the Zone 1 hosts two battery energy storage systems (BESSs), whose total available energy results equal to 452 kWh. Regarding the C-rate, a continuous charge/discharge is conventionally provided at 3C, whereas a discharge rate till 6C is available when the operating time is quite limited (i.e. seconds). To emulate even prohibitive load profiles (i.e. square-wave behaviour up to 2.5 MW as magnitude), two electronics loads are installed in Zone 2 to test and validate high-performance scenarios on the DC zonal system. To conclude the zones description, the third one is consid-

ered out-of-service for the purpose of this paper, although is equipped with a cooling system and electrical/data terminals. To ensure the power system aim, thus supplying high-demanding electronic load and providing buffering function with battery storage, the interfaces to zone 2, 3, 6, and 7 is provided by DC/DC power converters, as explained in [8]. A particularity of the proposed DC microgrid is the choice of electronics interfaces. In power electronics definition, the main characteristics to be pursued are affordability and widespread adoption. This constitute an important advantage of the proposed controlled system, where the electronics interfaces are not tailor made but based on standard-commercial solution. This means that the required flexibility and resilience are guaranteed only in presence of an advanced well-tested control architecture. In other words, each converter depicted in Figure 1 is composed of the integration of identical power electronics modules, whose combination assures both requested functionality (i.e. bidirectional DC/DC or AC/DC) and rated power. Each converter (from 1 to 8) is specified in Table 1, reporting rated power and number of modules. Each converter module has a 12 mF capacitor to the MVDC bus (i.e. 156 mF in total when the busbar is closed), fostering the system stability even with high-demand DC load connection. The consequent high current during short-circuit is conventionally managed by power converters through proper protection definition [32].

2.2 | Zonal DC control architecture

As previously mentioned, zonal power systems will require a specifically conceived control architecture to deliver their expected advantages. The IEEE developed a standard in this regard, which is the St. 1826, named “IEEE Standard for Power Electronics Open System Interfaces in Zonal Electrical Distribution Systems Rated Above 100 kW” [8]. The recommended control logic block diagram is shown in Figure 2a, considering a single power electronics converter as a building block for the

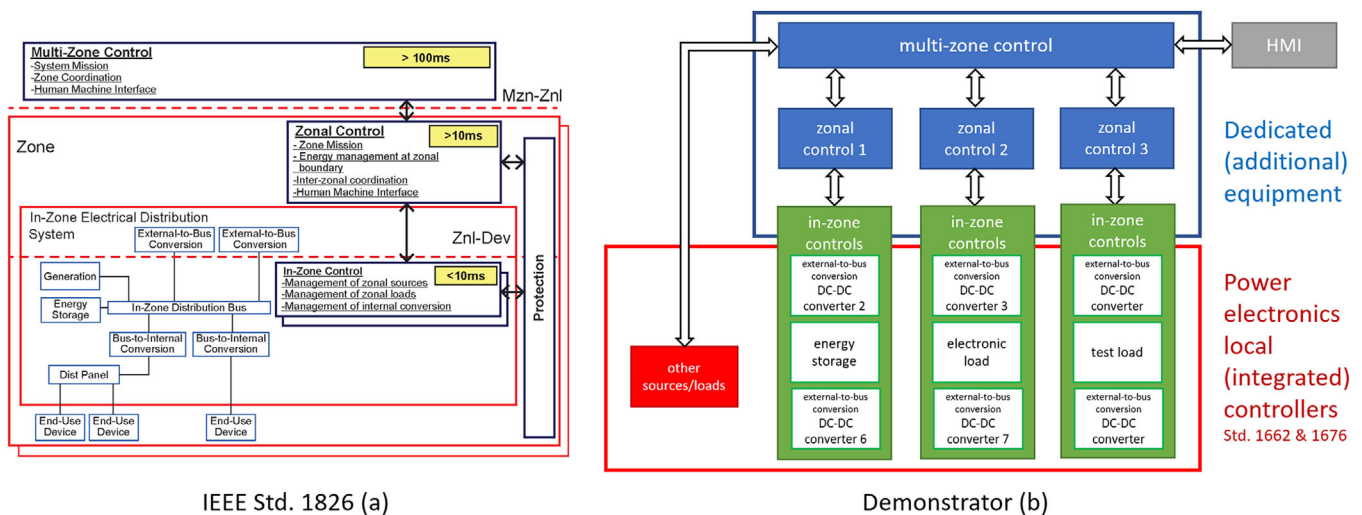


FIGURE 2 ZEDS control logic block diagram: IEEE Std. 1826 (a) and actually implemented in the testbed (b) [30].

entire power system (exploiting the PEBB – Power Electronics Building Blocks [33]—concept).

In this regard, the recommended diagram needs to be implemented in the power system design due to the specific needs each application may present. To this aim, the Authors worked on developing, building, and testing a real-scale DC zonal power system demonstrator, whose development and validation has been described in [30]. Concerning the control architecture, the multi-layer control architecture of Figure 2b is the result of such an effort. By comparing the two block diagrams of Figure 2, one can appreciate the similarities between the control logic block diagram of the standard [8] (Figure 2a) and the specific implementation made in the demonstrator (Figure 2b). Although differences are visible, some of which are determined by the fact that the Standard depicts a single converter while the diagram of the demonstrator applies a system-wide view, the same layers present in the Standard are depicted. Specifically, the following three layers are present: multi-zone control, zonal control, and in-zone control.

The top layer is the centralized multi-zone control: it determines the overall system mission, coordinates zones, and provides a human-machine interface (HMI) for the operator's supervision (for changing the system mission and providing a manual intervention in the control layers below). The middle layer is the zonal control: it is made of multiple functionally separated controllers (one for each zone of the system), and receives control signals from the multi-zone control. Its function is to translate the operational requirements coming from the multi-zone control into a configuration for the single zone, which is capable of delivering the set of functions required to perform the overall system mission. The latter is done through the setting of energy flow at the zone boundary, exploiting the active control capabilities of power electronic converters, and exchanging suitable health/status and command signals with both the above and below control layers. Inter-zonal coordination (i.e. a decentralized coordination function between zone that does not rely on the multi-zone control layer) is provided when applicable and needed. The latter enables autonomous operation of the zonal control in the absence of a higher coordination function, to achieve a stable operating point. The control layer closer to the power and hardware is the in-zone control. This layer is made by the field control systems of each single power converter, which must include the capability of operating also in absence of communication with the above layers. This layer performs several functions by means of controllers directly integrated into the equipment (e.g. the converters current/voltage control loops). The zonal control layer controls the parameters and setpoints of such internal control functions, thus enabling equipment coordination and ensuring the zone's correct operation (with the ultimate goal of meeting the multi-zone defined mission). All these layers have been implemented through several elements/components in the demonstrator (Figure 2b), exploiting the integrated control functions of the power converters where possible (in-zone control), and installing dedicated equipment for the rest (multi-zone and zonal control layers). The former integration is made possible by the converters having an inter-

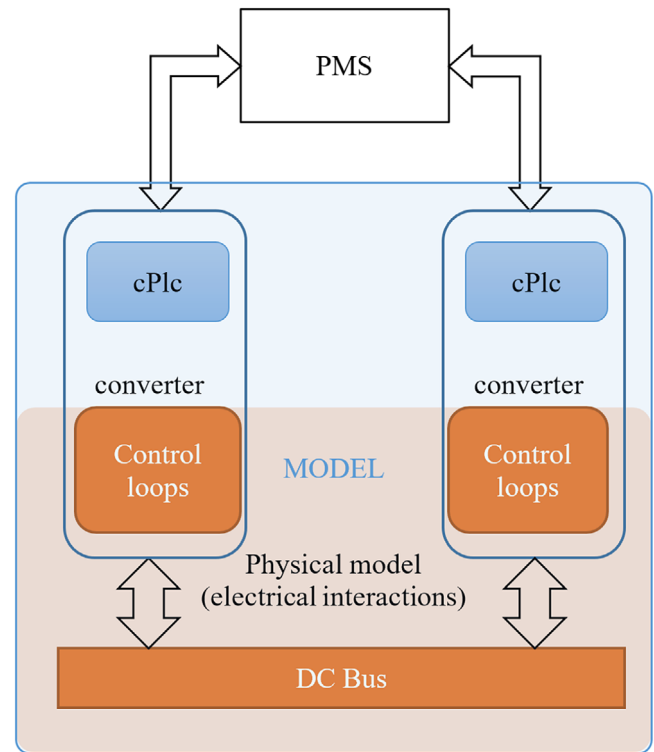


FIGURE 3 Zonal DC distribution control layers [34].

nal control structure compliant to IEEE Stds. 1662 [12] and 1676 [13].

To achieve the aims of this paper, it is required to model the power system control infrastructure in the HIL systems, along with the power electronics and other power equipment. Following the above mentioned zonal control architecture, different control layers thus need to be specifically modelled. To this aim, the in-zone control layer has been implemented into the converters' models, using their control loops, while the zonal and multi-zone layers have been implemented with dedicated simulated equipment (Figure 3). Specifically, for the purpose of this paper, the previously mentioned PMS provides both the zonal and multi-zone control functions, integrating all the related control loops and logic.

2.3 | System modelling

To develop the digital twin of the power system in Figure 1, using the first HIL approach based on an open-source real-time OS, it has been decided to exploit nonlinear average value models (AVMs). These models are obtained starting from the system equations and are implemented as block schemes in Simulink, then embedded in a real time simulator to allow for the connection with an external controller. A detailed description of the modelling activities is included in [30], while the development of the open-source real-time simulator is discussed in [34]. Conversely, the second digital twin implementation is based on the idea of mixing AVM and circuit-level models, exploiting the Typhoon HIL hardware and software platform.

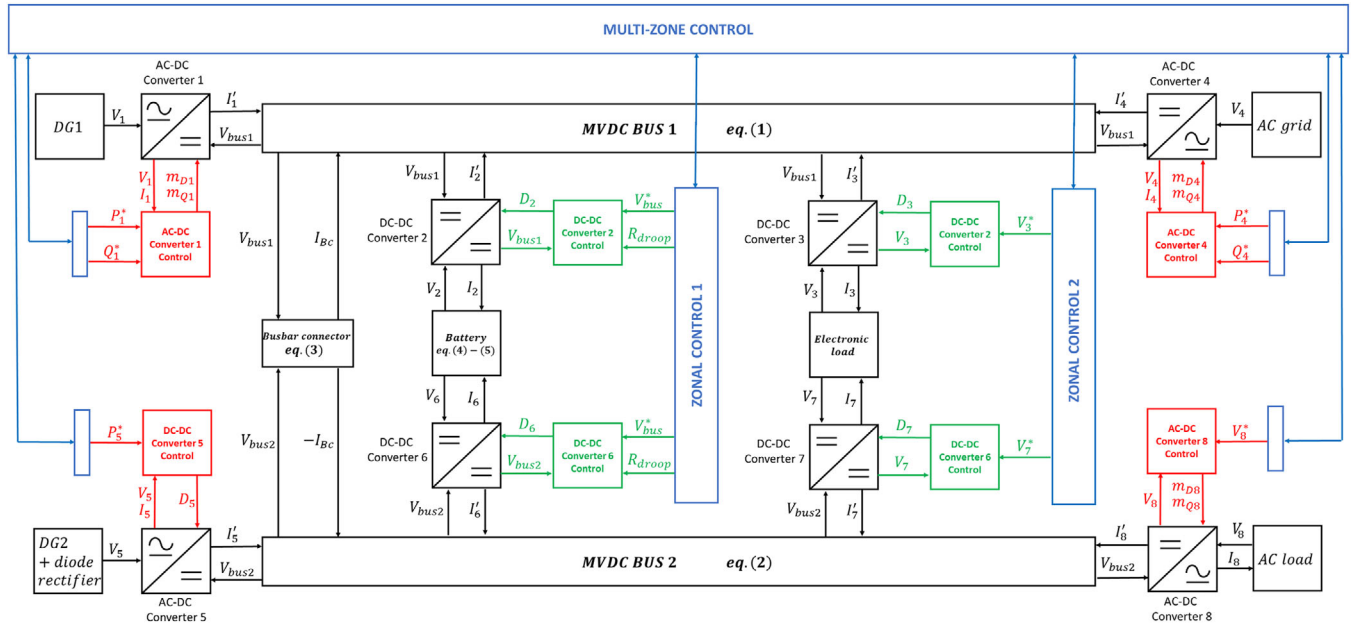


FIGURE 4 Block representation of complete MVDC ZEDS, modelling power and control systems [30].

The overall block representation of the Figure 1 power system and its control is depicted in Figure 4, where the black boxes represent the power system components, while the red, green and blue ones are used for the control sections. To perform the real-time analysis, Matlab-Simulink is adopted to implement the nonlinear average value model (AVM), where the discrete-time integration is performed with a fixed time step of $10 \mu\text{s}$. Five important assumptions are initially defined to simplify the modelling, as follows: 1) the switching on power converters is neglected; therefore, their dynamic behaviour is expressed by AVMs; 2) an ideal-constant voltage source is used for modelling the input from AC grid; 3) linear resistive elements are adopted to model both electronic load and load bank; 3) two ideal-variable voltage sources are representative of diesel generators (DGs); 4) in DC–DC voltage-controlled converters (Zone 1 and Zone 2), the current control loop dynamic is assumed to be negligible when the transients are on the order of 1 s. Regarding the last point, it is better to clarify the methodology adopted in conceiving the models. In case the transients settle in about 1 s (i.e. high-bandwidth dynamics), the undisturbed operation of DGs is represented by ideal constant voltages. On the other hand, in case of low-bandwidth dynamics (i.e. transients concluding in a time larger than 1 s), a predetermined ramp rate on interface converter is adopted for the regulation of DGs output power.

The zonal MVDC microgrid is based on two buses (Figure 4), whose voltage is modelled in Equations (1)–(3). Such bus voltages are determined as a function (3) of I_k , converters' output currents (Table 1) and I_{Bc} bus connector current. For what regards the Zone 1, the battery is simply modelled (4) as an open-circuit voltage $V_{OC,k}$ and a resistance R_{bk} . This representation is effective in identifying the V_k input voltage for converters 2–6. The V_k represents the voltage on a battery when interfaced with a load/source, while the battery func-

tioning in open-circuit case is given by the $V_{OC,k}$ open-circuit voltage (OCV). Evidently, the last term behaves as a function of the state of charge (SOC), whereas the OCV-SOC is derived by interpolation from the battery's datasheets. The SOC is then obtained [35] by Equation (5). Here, the battery capacity is expressed by $C_{b,k}$, the conversion factor from hours to seconds is named k_b and I_k models the inductor current in the k th converter filter. Based on the literature [36, 37], the battery model is identified as in Equations (4) and (5). Although its simplicity (i.e. phenomena like battery aging, hysteresis or Coulombic efficiency are neglected as they are not relevant for the digital twin's aim), it is considered sufficient to proficiently analyse the dynamic behaviour in a ZEDS. Also, the control logics are not considered in the converters models equations. Specifically, reference [38] is adopted in the modelling of DC–DC converters, whereas the AFE converters models come from [39]. By considering all the hypotheses and mathematical equations, the complete model of zonal MVDC microgrid (Figure 1) and its control infrastructure (Figure 2b) is visible in Figure 4. In this representation, the power components are depicted in black while the control layers are represented by different colours (i.e. blue, green, red).

The control blocks' inputs are the setpoints imposed by upper controllers (star marked) and the closed-loop controlled variables. The control signal for the power converters, thus the control blocks outputs are the duty cycles for DC–DC converters or the modulation indices for AFE interfaces. The controlled functioning of each converter is detailed in Table 1 where the specific control mode (i.e. power, bus voltage, load voltage, voltage and frequency) is shown. As the BESS converters are both in charge of regulating the same bus voltage, the droop control functionality on the DC grid is utilized to decouple the control loops while properly sharing the power among the electronics converters [40–42]. These droop coefficients are tuned in

accordance with common practices on DC microgrids [43], therefore sufficiently small to avoid large drops on the bus voltage in high-demanding load scenarios.

$$\left\{ \begin{aligned} pV_{\text{bus1}} &= \frac{1}{C_{\text{bus1}}} \left[\sum_{k=1}^4 I'_k + I_{\text{Bc}} \right], & C_{\text{bus1}} &= \sum_{k=1}^4 C_k \end{aligned} \right. \quad (1)$$

$$\left\{ \begin{aligned} pV_{\text{bus2}} &= \frac{1}{C_{\text{bus2}}} \left[\sum_{k=5}^8 I'_k - I_{\text{Bc}} \right], & C_{\text{bus2}} &= \sum_{k=5}^8 C_k \end{aligned} \right. \quad (2)$$

$$pI_{\text{Bc}} = \frac{1}{L_{\text{Bc}}} [V_{\text{bus1}} - V_{\text{Bc}} - R_{\text{Bc}} I_{\text{Bc}}] \quad (3)$$

$$V_k = V_{\text{OC},k} (\text{SOC}_k) - R_{\text{b},k} I_k \quad (4)$$

$$p\text{SOC}_k = -\frac{1}{\kappa_b C_{\text{b},k}} I_k \quad (5)$$

The first digital twin implementation was developed using the Linux real time application, and only AVMs are used for the power system simulation. In contrast, in the second digital twin implementation the Zone 2 converters and electronic load are developed using switching model on the Typhoon HIL platform. The Zone 2 converters, namely DC–DC 3 and DC–DC 7 are two phase interleaved converters that are in charge of controlling the voltage on the electronic load. For this purpose, a PI controller is used, as in Equation (6), in which the terms K_{pV} and K_{iV} are the proportional and integral gains of the PI controller, while the V_{load}^* is the reference voltage for the load. The output of the voltage controller is the reference current for the converter, I^* , which, when divided by the number of phases (in this case two) becomes the input of the PI current controller (K_{pI} and K_{iI}) of each converter leg. The current controllers, Equations (7) and (8), provide as output the voltage reference, u_a and u_b , for the PWM, which generates switching signals in order to obtain a 180° phase shift between the currents of phase a and b. The effect of this current interleaving action is shown later in the results section.

$$I^* = \left(K_{pV} + \frac{K_{iV}}{p} \right) \cdot (V_{\text{load}}^* - V_{\text{load}}) \quad (6)$$

$$\left\{ \begin{aligned} u_a^* &= \left(K_{pI} + \frac{K_{iI}}{p} \right) \cdot \left(\frac{I^*}{2} - i_a \right) \end{aligned} \right. \quad (7)$$

$$\left\{ \begin{aligned} u_b^* &= \left(K_{pI} + \frac{K_{iI}}{p} \right) \cdot \left(\frac{I^*}{2} - i_b \right) \end{aligned} \right. \quad (8)$$

3 | DIGITAL TWIN OF A DC ZONAL DISTRIBUTION SYSTEM

The implementation of a digital twin of the power distribution in Figure 1 makes it possible to expand the capabilities of the zonal demonstrator, offering a safe environment to test either new control architectures or new loads and storages. This digital twin is thus exploitable to perform de-risking activities before new installations on the physical demonstrator and serves as a

tool for personnel training activities. The initial solution for the digital twin development was the usage of average value models (AVMs), which are quite easy to implement, do not require detailed data and can represent the dynamic behaviour of the power system. Indeed, using AVMs a first solution for the digital twin implementation was proposed in [34] using an open-source solution. However, if more complex P-HIL emulations are to be performed, other solutions need to be investigated to be able to supply properly the power interfaces connected to the power system emulator. The idea has been to combine the AVM and switching models. A portion of the power system is simulated using AVMs, while the portion of the systems that will be connected to a possible external physical load is to be emulated using switching models. The detailed switching models are built on the Typhoon HIL 604 platform, which is particularly suitable for the development of C-HIL and P-HIL configurations.

3.1 | Implementation on real-time application interface

In this study, the RTAI open-source Linux kernel, known for its real-time performance capabilities, is used. The real-time characteristic of RTAI is achieved through modifications in interrupt handling, which are detailed in [29]. RTAI has found applications in various contexts where real-time execution of control algorithms is essential. The main issue in adopting an RTOS for real-time devices is the scheduling jitter of the system: it determines the minimum scheduling time of the control algorithm that can be implemented on the specific device. For instance, in [44], researchers examined the use of RTAI for voltage control devices in transmission networks. In [45], RTAI was employed for HIL (Hardware-in-the-Loop) simulation of diesel engines, while [46] and [47] showed applications of RTAI in motion control. Performance metrics of a Linux-based real-time system are discussed in [48], and these measurements were conducted under different operating conditions. Notably, scheduling time jitter strongly relies on real-time I/O operations performed on I/O boards connected to the PCI bus. In this work, RTAI has been used to build a real-time model of the electrical network, facilitating communication between simulated devices and the PMS (power management system) via Modbus/TCP in non-real-time mode. This approach eliminated the need for exchanging values through wired analogue or digital cards. Consequently, the scheduling time jitter exhibited low variability, and the latency was minimal. As a result, it was possible to execute the digital twin with a fixed step of 20 μs , which yielded high accuracy.

Since there was no need for wired inputs and outputs, and being able to limit all communications to the Modbus/TCP protocol (which is not executed in real-time), a very low sampling time jitter was obtained. In Figure 5, the actual value of the sample time at the start of each simulation cycle is shown. During a period of 10 s (which means 500,000 samples) the minimum sample time registered was 13 μs , while the maximum was 28 μs . A magnification of the data shows that the deviation is quite low. The probability density function of the sample time shows

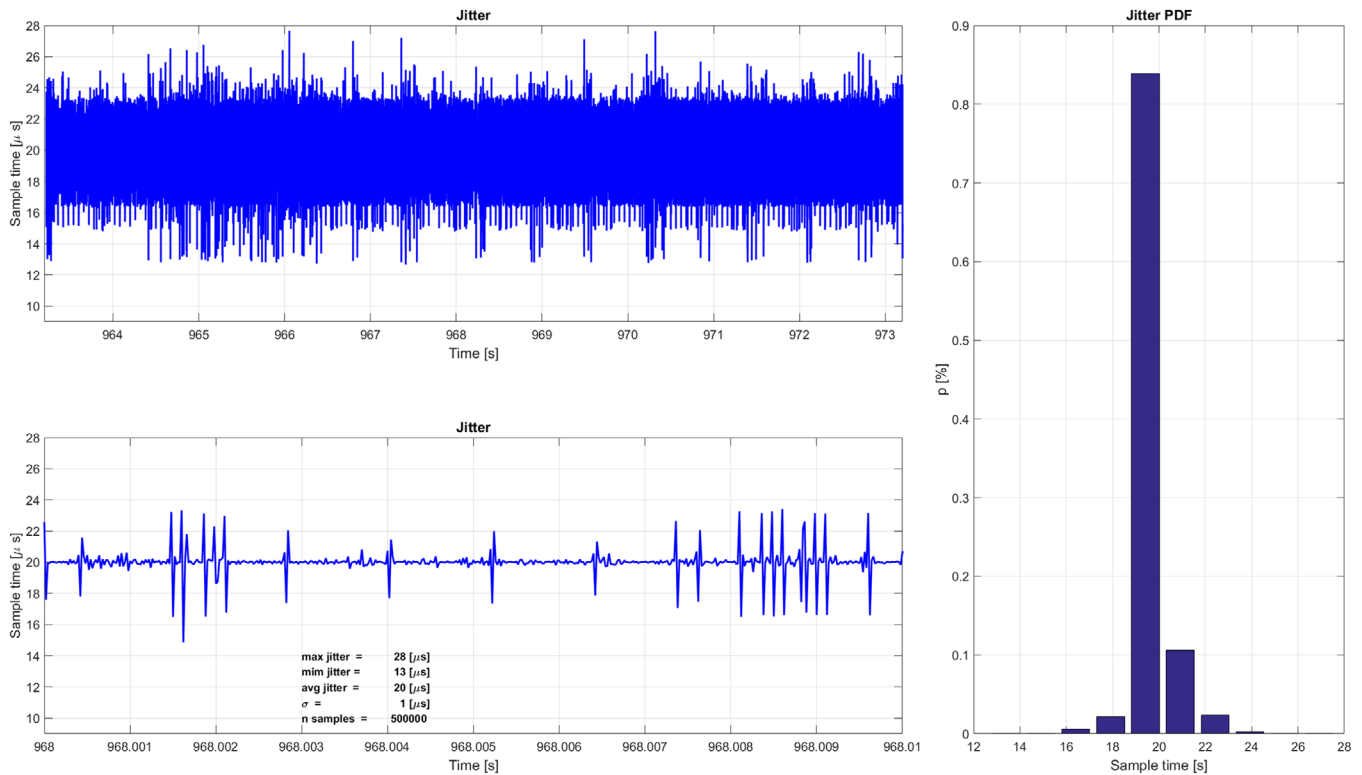


FIGURE 5 Jitter measurement: actual value of the sample time of the starting of each simulation cycle (top left), magnification of the latter (bottom left), and probability density function of the sample time (right).

that more than 80% of the samples have a jitter less than 5 μs . The jitter data shown in Figure 5 thus attests that real-time execution provides the required performance to execute the digital twin with an acceptable accuracy without losing the real time capability.

The whole simulator architecture is shown in Figure 6. The mathematical model of the electrical network has been developed in the Matlab Simulink environment, which has been subsequently translated into C code and compiled for the X86 platform (green box). The model includes coding for all the converters and their connections to the DC bus. A single real-time process simulates the network with all the converters, employing a fixed step of 20 μs . In the actual system, the converters are controlled by the PMS through Modbus/TCP-based communication. In the digital simulator the communication implementation of the Modbus protocol running on all static converters is executed in non-real-time (yellow box). The IP network architecture is reconstructed as in the real power plant (with the same IP addresses).

As in the real plant each drive possesses a CPU with a network card configured to communicate with the PMS using an IP address and the Modbus/TCP protocol. Similarly, in the simulator each mathematical converter model has its own interface with an IP address matching that of the real system. Additionally, a separate communication process, operating at a lower priority, simulates communication via the Modbus/TCP protocol. To implement the protocol, the libmodbus library [49] has been used.

Two other processes in the simulator simulate battery status and resistive load communications. In the real system, the battery state involves data exchange using the CANBUS protocol with a PLC acting as a gateway. The PLC then communicates with the PMS via UDP messages sent every 20 ms. Similarly, in the simulator the communication occurs unidirectionally towards the PMS, with UDP packets sent every 20 ms. The resistive load state in the current model is simulated with a fixed configuration. The complete simulator runs on a Pentium CPU dual core G4400 at 3.30 GHz (Skylake architecture) with a Linux Ubuntu 64 bit patched with RTAI. RTAI 5.1 is one of the latest releases of the RTAI patch and has been installed on a Ubuntu version 16 to use a kernel version suited for the patch.

3.2 | Communication protocols

The digital twin of the plant described in this paper consists of two main components: the mathematical model of the electrical DC grid (including the static converters) and the data communication network through which measurements, control actions, and local control references are transmitted. Communication protocols play a crucial role in enabling devices to interact with each other to achieve the desired operation. The aforementioned communication protocols are the most commonly used in electrical networks. They facilitate the transfer of data from the converters to the main controller (the PMS), which processes the setpoints and transfers them to the static

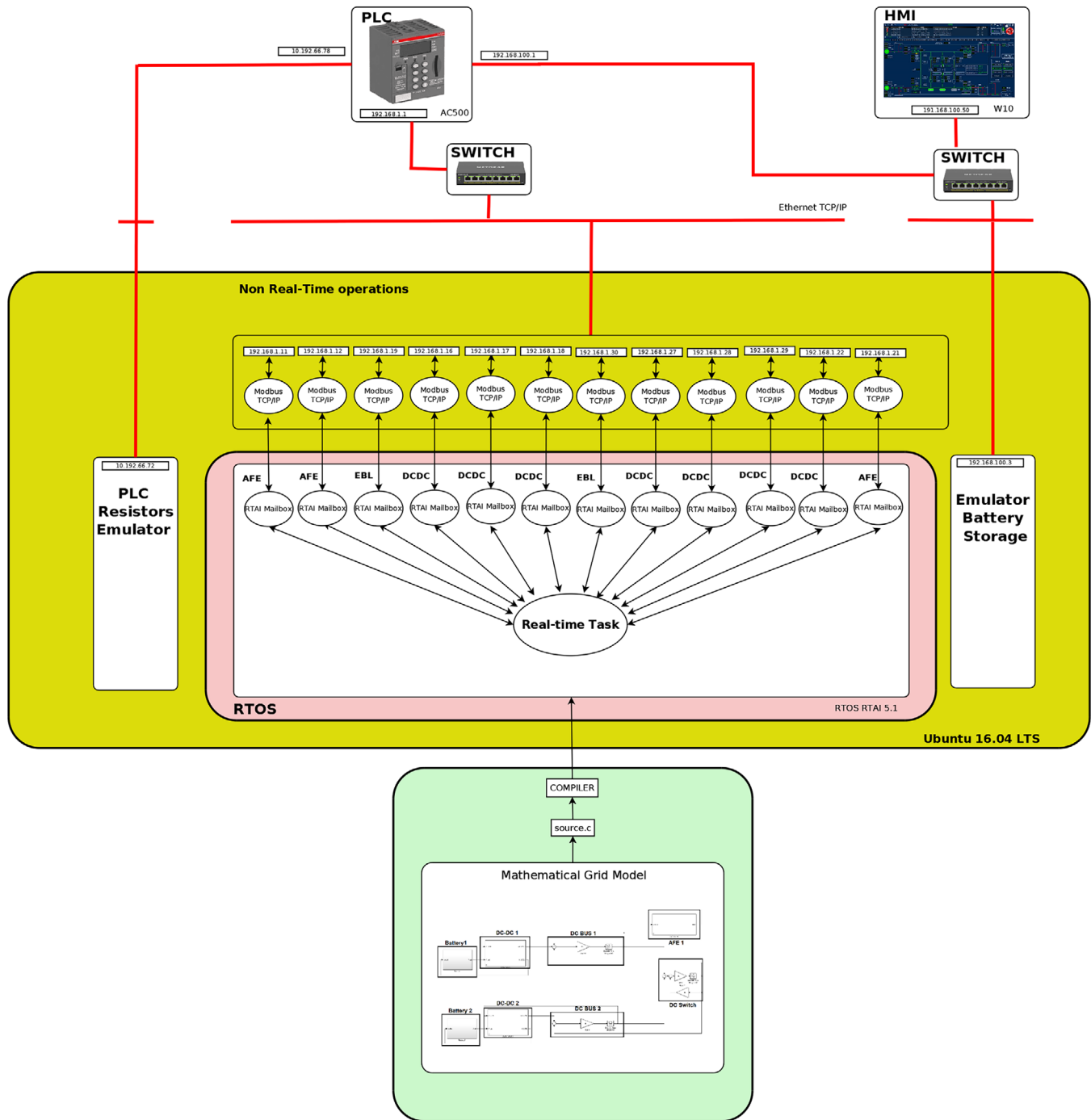


FIGURE 6 HIL architecture: compiled mathematical model (green box), running in real-time on a Linux operating system after compilation in C (pink box).

converters. In the digital twin, the communication of this data from the PMS to the converters and switches is simulated to closely resemble reality. While the standard [8] recommends using communication based on the IEC 61850 standard, the Modbus/TCP protocol was utilized in this study for practical reasons. This protocol is widely used in industrial automation and naval power systems. Modbus, developed in the late 1970s, originally relied on serial communication at the physical level. It operates above layer 4 of the ISO/OSI stack. For the lower levels, two options are available:

- Modbus RTU: Modbus packets are transferred through a serial network using RS-232 or RS-485 cables.
- Modbus over TCP/IP: Packets travel through the TCP/IP stack.

The system described in this study employed the IP layer. Each converter connected to the network is assigned an IP address, which facilitates packet routing within the network. The Modbus protocol follows a client-server model, enabling one-way communication. In the real plant, the PMS acts as the

client and polls the Modbus servers implemented within each static converter's controller. Each converter is assigned an IP address and listens on port 502 to respond to PMS requests. These requests primarily involve fetching values of variables measured by the converters, such as voltages and currents, as well as storing reference settings in the converter's writable registers. A Modbus device, referred to as a server, follows a simple architecture consisting of read-only and read-write registers.

To enable communication between the logical and mathematical model of the distribution grid and the PMS, it is necessary to develop a program that manages this communication. In the actual network, each converter already has a program integrated into its logic that is compatible with the Modbus protocol. This program needs to perform the following tasks:

- Receive and transmit data from the model
- Transfer the commands from HMI (through the PMS) to the model
- Be compatible with the Modbus TCP/IP protocol in order to talk to the PMS implemented by a commercial PLC.

To simulate the communication module of each converter, a multi-thread approach was adopted. Three processes operate simultaneously: one thread manages the Modbus communication, another thread allows the real-time execution of the mathematical model to export data into a shared memory accessible to the Modbus thread, and a third thread enables the model to receive commands from the PMS through Modbus communications. This multi-threaded program was written in the C language and extensively utilizes the open-source library Libmodbus [49], version 3.1.7. This library provides functions that enable communication via Modbus TCP/IP.

In the digital twin, an IP address is assigned to each converter, and a communication server running the three described threads is implemented. A portion of the communication server executes in real-time to interface with the real-time executed model, while another portion executes outside of real-time (specifically, the Modbus communication part). For each converter, there is a configuration file that describes the registers used by that specific converter. With the information in the configuration file, a shared memory is allocated, which contains all the converter's registers. The PMS polls all the converters at a frequency of approximately one Hertz, requiring around fifteen 32-bit registers (fewer for EBL switches). Each ModbusTCP read or write operation has a total execution time ranging from 20 to 100 ms. These latency times are similar in both the real plant and the digital twin. Commands are dispatched sequentially from the PMS to the converters, experiencing non-deterministic delays in the tens of milliseconds range. These small delays can cause settling times in the power output of the batteries, as seen in Figures 10 and 11.

In synthesizing the converter models, both the mathematical model of the device's electrical behaviour and the logic model implemented in the converter are considered. Finite state machines from the Simulink Finite State Machine library are utilized for this purpose. The logic implemented in the converters is not always accessible as the converter software is not publicly

available. In such cases, the logic is obtained through external analysis (black box) of the converter.

The utility of a model at average values, communications architecture, and protocols is manifold

- By interfacing the PMS controller with the model, it becomes possible to verify the accuracy of all potential interactions between the PMS and the system. Command sequences can be tested, and simulation allows for checking delay times that may exist in the real system.
- The model enables the simulation of cybernetic issues within the system. For instance, it allows for the simulation of cyber-attacks on the data network [50], as well as the effects of non-fraudulent errors in the data network.
- It provides the ability to assess the impact of changes to the computer network structure, such as protocol replacements (at the physical level or at levels three and four of the ISO-OSI model, or even at the application level), network segmentation into different subnetworks (including the presence and simulation of gateway devices between networks).
- The digital twin can be employed for operator training activities, facilitating comprehensive interaction with the interface.

It is relevant to notice that there are some critical points related to the use of the above-described approach for building a digital twin using an RTOS. The model simulates the behaviour of the electrical DC grid and of 12 static converters. Each controller essentially has an IP address. Other types of simulations use to simulate also the IP network itself which, in this work, is instead implemented in an almost complete way. For the simulation of the IP network, several IP addresses are assigned to a single network card. This can lead to an overload of IP packets on a single physical interface which can lead to slowdowns that do not occur in the physical plant. The possibility of having several physical network cards should possibly be considered in order to distribute the IP addresses of the various converters.

3.3 | Implementation on C-code

An upgrade of the previous digital twin is proposed in this paper. The idea is to start from the AVM models of the open-source implementation and combine them with the commercial emulation platform Typhoon HIL 604. This platform allows for easy development of switching models of the power converters and has inherent real-time emulation capabilities. As already done with the RTAI implementation, the Simulink models of the power system components are compiled to obtain C-code; this code is then integrated into the Typhoon environment using the Advanced C function block. This block can communicate with the Typhoon environment only with input and output signals. Indeed, to connect the power sections of the Typhoon and Simulink models, the signal-controlled sources and voltage/current measurements are used. This concept is clarified in Figure 7, which represents a general idea of what the

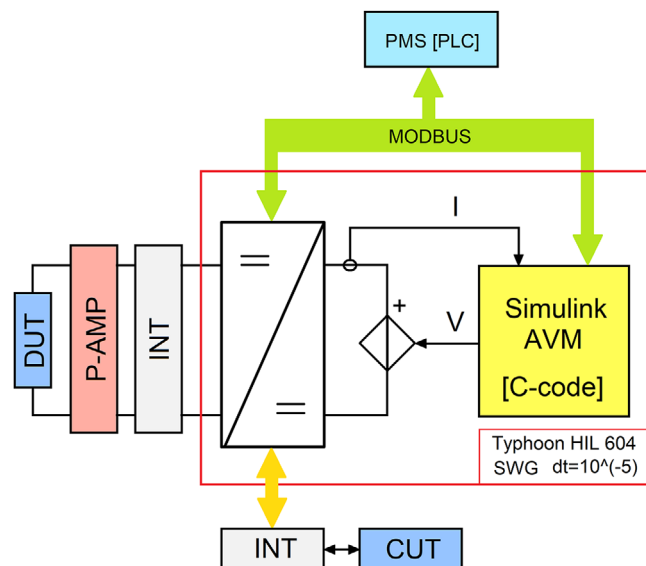


FIGURE 7 C-code implementation.

C-code implementation is: part of the power system is simulated using the C-code coming from the Simulink model, and this block sends a control signal to the controlled voltage source implemented in Typhoon. The controlled source is interfaced with a converter modelled in detail (switching) in Typhoon HIL. Meanwhile the converter input current is measured, and a feedback signal goes back to the C-code block to close the loop. This combination of models can be used to emulate the power system in a more versatile way, allowing for the interconnection with an external controller, both via Modbus or by directly connecting the Typhoon input and output pins to a possible controller under test (CUT). Another possibility, as shown in Figure 7, is to interface the emulated power system to a device under test (DUT) through a power amplifier, reaching a power

hardware in the loop (P-HIL) setup. In this setup, the AVM part of the power system is simulated using a $10 \mu\text{s}$ time step, and the same is done for the switching part.

The setup used for this work's case study is represented in Figure 8. The portion of the power system implemented using switching models is surrounded by the red line. It includes two DC–DC converters and the electronic load that they supply. These two converters are two-phase interleaved DC–DC converters and are modelled in detail in the Typhoon environment, while the electronic load is simply modelled with a resistor. The rest of the power system, surrounded by the green line in Figure 8, is modelled in Simulink as described in Subs. II-C and then compiled in C for the integration into the emulation platform. The yellow boxes represent the interface between the two models, AVMs and switching ones. There are two controlled voltage sources and two current sensors that make it possible to interface the two models, as shown in Figure 7. The compiled Simulink model sends the bus voltage measurement, driving a signal-controlled voltage source, one for the bus 1 and one for the bus 2. In the meantime, the current at the output of the two converters implemented in Typhoon is measured, filtered, and sent to the Simulink model. From the overall power system control point of view, for this C-code implementation, the connection with the actual PLC of the zonal power system is not yet developed. For now, a simplified-yet effective version of the PMS is conceived and controls this particular setup directly from the Typhoon HIL SCADA.

4 | DIGITAL TWIN TESTING ON AN EXPERIMENTAL CAMPAIGN

The two digital twin implementations proposed in this paper are now compared to the actual experimental data. The test is performed with the busbar connector closed, the AC–DC

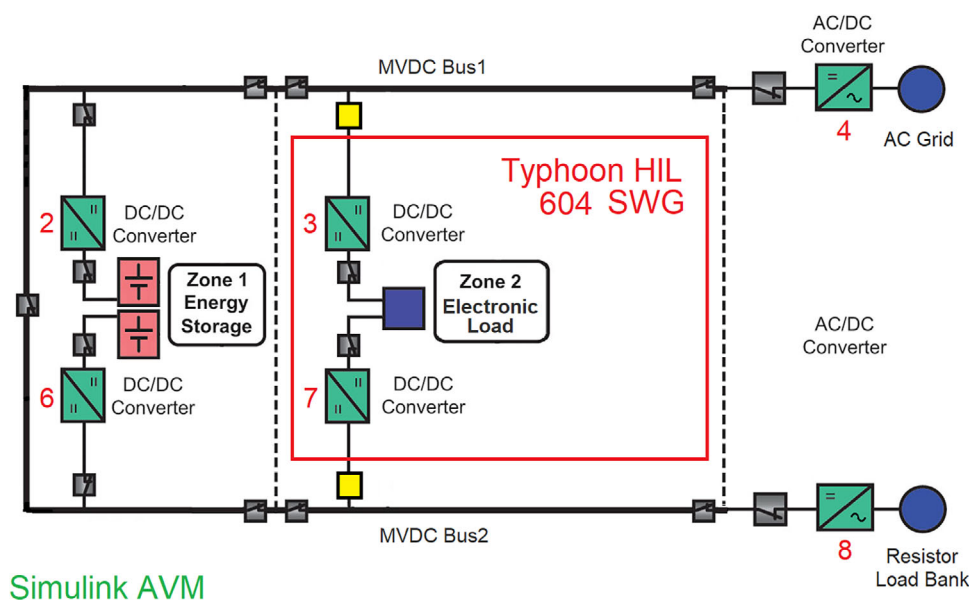


FIGURE 8 C-code implementation simulation setup.

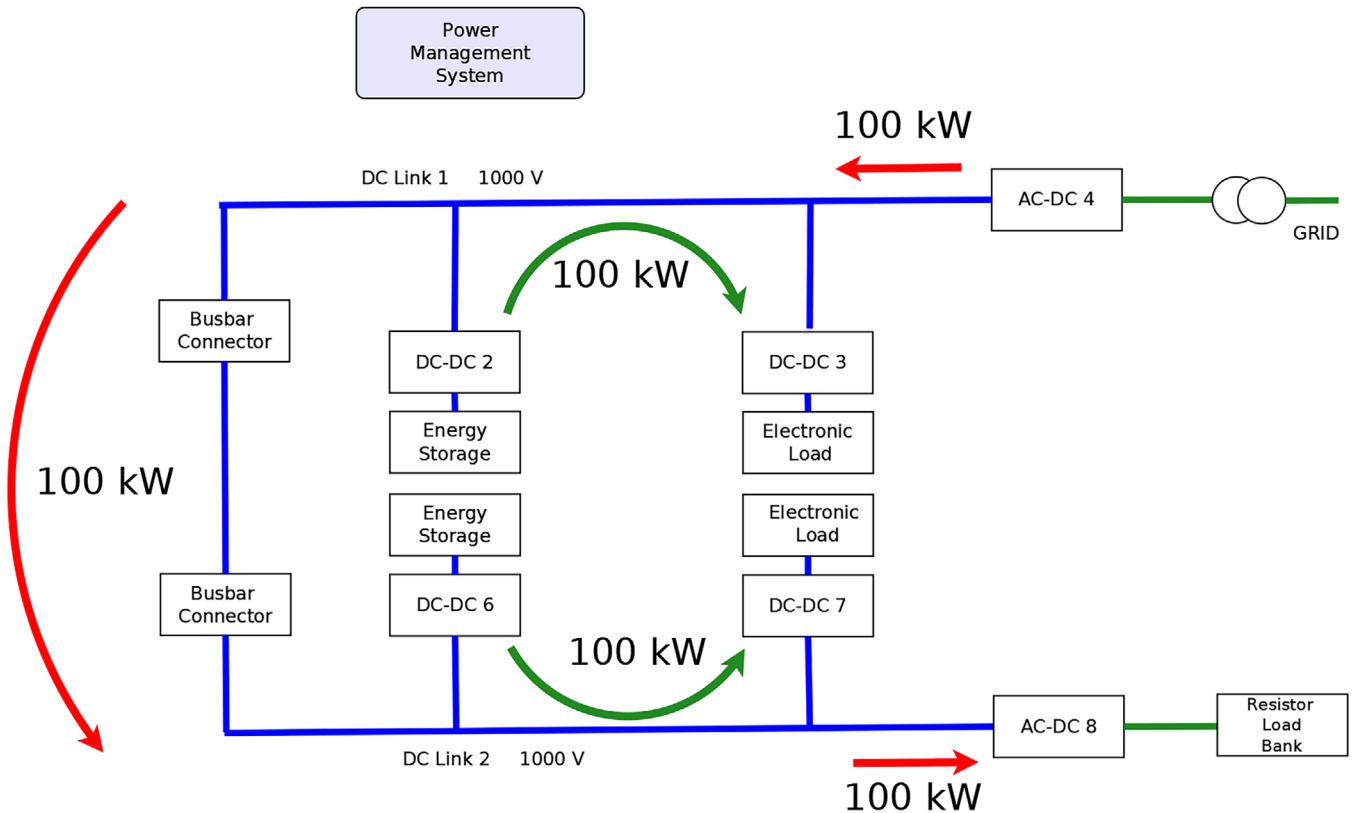


FIGURE 9 Flows of power on the test on the digital twins.

converter 4 is supplying 100 kW of power, and the AC–DC converter 8 requires approximately 100 kW (slightly less considering the losses, but for the sake of simplicity, the paper later always refer to 100 kW). The perturbation under analysis is the sudden connection of 200 kW of step load in the Zone 2; this load is then maintained for approximately 20 s. During this transient, the Zone 1 batteries are supplying the load step, and their converters are regulating the bus voltage. To give a visual idea of the test performed, Figure 9 provides the power flows in the power system of Figure 1 during the above described test. In Figure 9, the red lines represent the power delivered from the AC grid to the resistor load bank, while the green line identifies the power that the two batteries supply to the electronic load through the DC–DC 2 and DC–DC 6 converters during the load step application. No energy is drawn from the diesel engines (as their converters are disconnected). This same test is performed on the MW-scale demonstrator of Figure 1 and on the two digital twin implementations presented in Section 3; the results are discussed in the following sections. Although this paper demonstrates the digital twin capability in analysing a small-power example, the same approach followed in this work was adopted also in a large power case. In this regard, the paper [30] indeed shows how the mathematical modelling based on AVMs results efficient also in reproducing the measured transients of a MW case. This work constitutes the final effective verification on the capability of digital twins based on average value modelling. Regarding the study case, all the data are

reported in Table 1 and in [30], with a particular attention on controlled DC grid and measurement systems.

4.1 | Comparison of RTAI simulation and experimental data

The implementation with RTAI has allowed for the construction of a real-time simulator of the entire network that responds to the commands of the original PMS sent via the data network using the Modbus protocol, exactly as in the real plant. It was therefore decided to carry out a comparison between the simulation and the real system during the exemplifying test described above and shown in Figure 9. The operation is carried out by acting on the commands offered by the PMS interface; a load of 200 kW is commanded on the electronic load, which the PMS divides equally between the DC–DC 3 and DC–DC 7 converters. The experimental power transients of both the electronic load and battery converters are shown in Figure 10, while their simulated counterparts are in Figure 11. The step has a steepness that brings it to full value in about 20 ms. The two batteries divide the load equally. Small variations can be noted in the power drawn from the batteries, which depend on the difference in state of charge and on the fact that the commands sent via Modbus to the two converters are inevitably sent sequentially by the PMS and therefore at different times, although very close. The variations in the power delivered by the two batteries

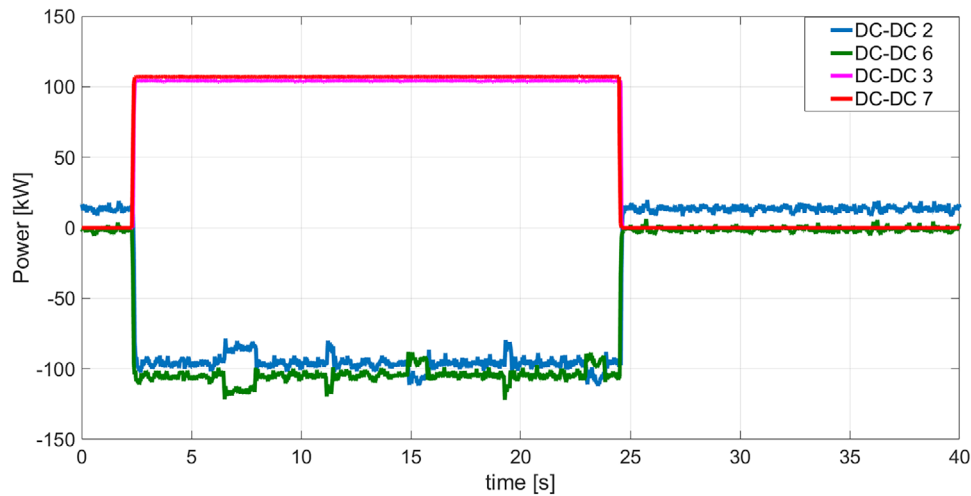


FIGURE 10 Power transients of battery and electronic load converters, experimental data.

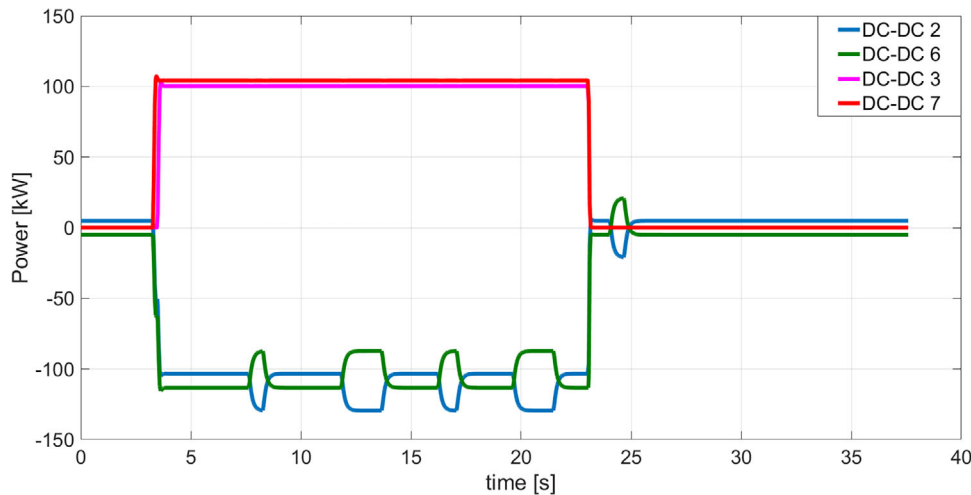


FIGURE 11 Power transients of battery and electronic load converters, C-HIL implementation on RTAI.

are also visible in the simulation while maintaining the power delivered by the zone constant. Even in the C-HIL simulation, the commands sent in time sequence from the PMS arrive with the same small random delays to the converters. These delays are due to the Ethernet physical protocol and the Modbus application protocol on the IP network. As can be seen from the Figure 12, the two converters act as a zone, and although they operate at different times, Zone 1 delivers a constant power, which is received by Zone 2. Figure 13 shows the RTAI simulation data of the zone's power. In Figures 14 and 15 the value of the bus voltage is shown for the experimental and simulated setups, respectively. The last transients in Figures 16 and 17 show the power at the AC-DC 4 and AC-DC 8 converter interfaces, which remain constant during the entire test, both in the experimental test (Figure 16) and in the RTAI implementation one (Figure 17). The experimental transients show the ripple of the converter's electrical parameters (i.e. voltage and power), while clearly the AVMs results are perfectly clean. However,

the general system behaviour is accurately reproduced, this is particularly visible in Figure 10 vs Figure 11, where the delays of the PMS signals transiently change the operating points of the DC-DC 2 and 6 converters, both in the experimental and RTAI simulation. In general, the RTAI digital twin performance are satisfying and are capable of reproducing with the needed accuracy degree the system behaviour.

4.2 | Experimental data versus C-code data

In this subsection, the experimental transients are compared with those from the C-code implementation, these results are included in the Figures 18–23. The column on the left includes the experimental data, while the column on the right represents the C-code implementation data. At the beginning of the test, the system is at steady state; the AC-DC converter 4 is supplying the system with 100 kW of power, while the AC-DC converter

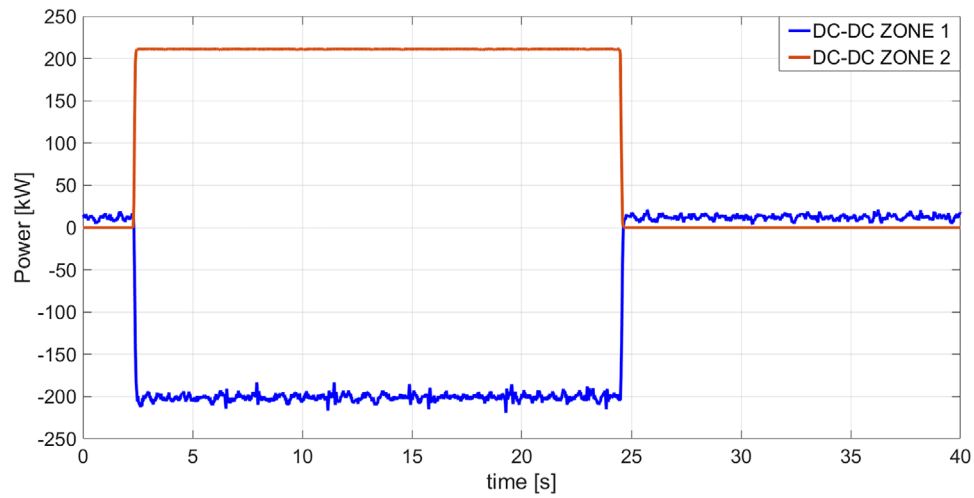


FIGURE 12 Power transients of Zone 1 and Zone 2 converters, experimental data.

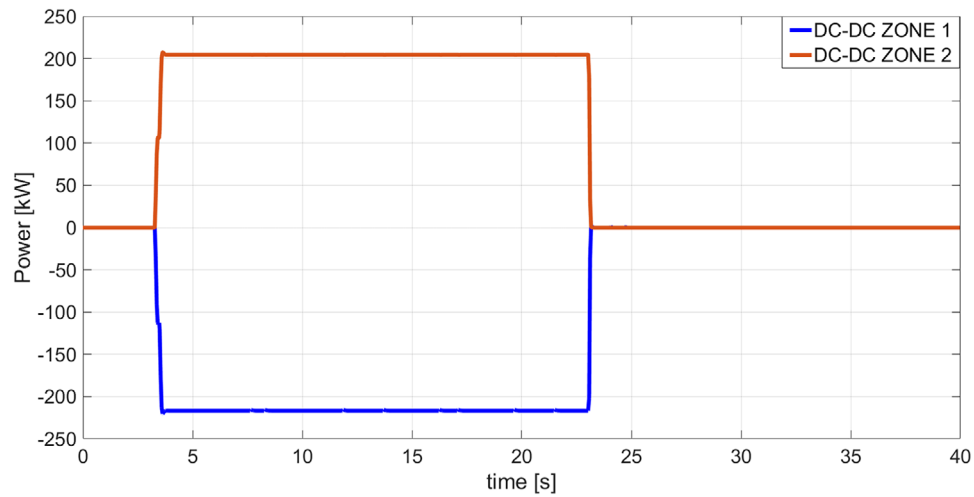


FIGURE 13 Power transients of Zone 1 and Zone 2 converters, C-HIL implementation on RTAI.

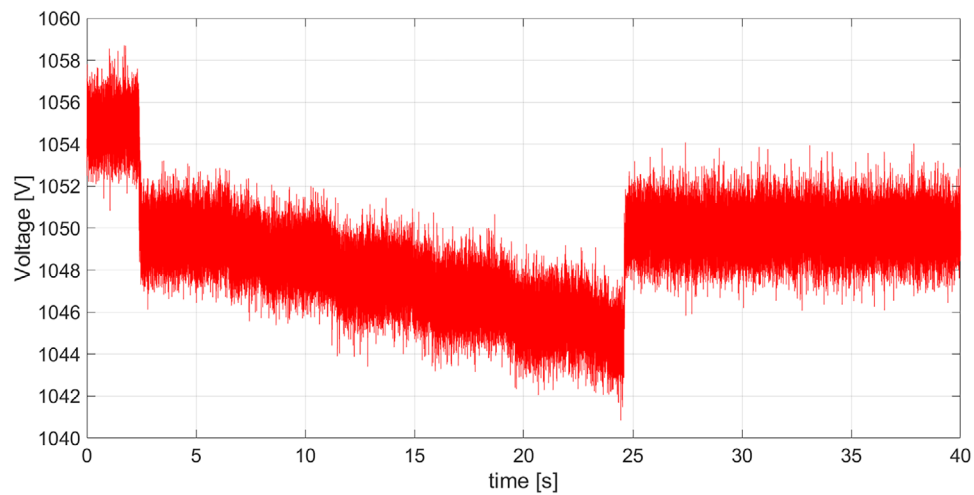


FIGURE 14 Bus voltage transient, experimental data.

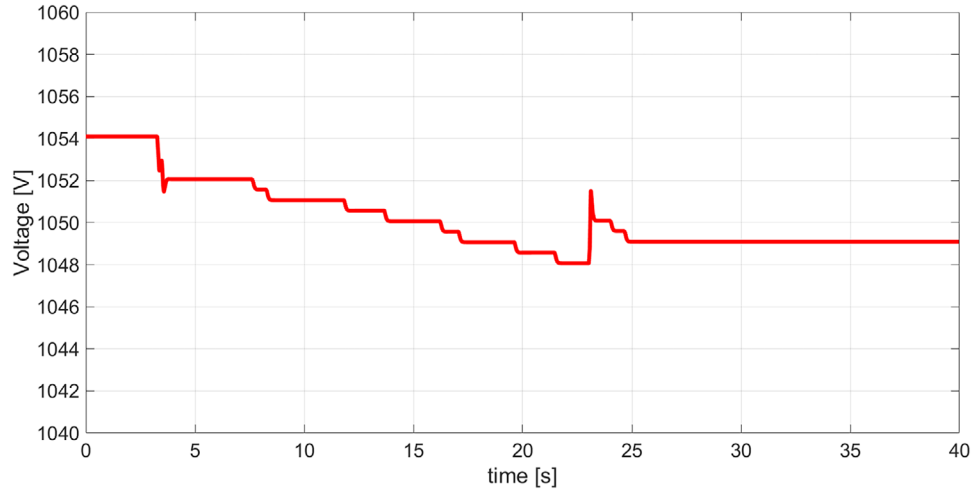


FIGURE 15 Bus voltage transient, C-HIL implementation on RTAI.

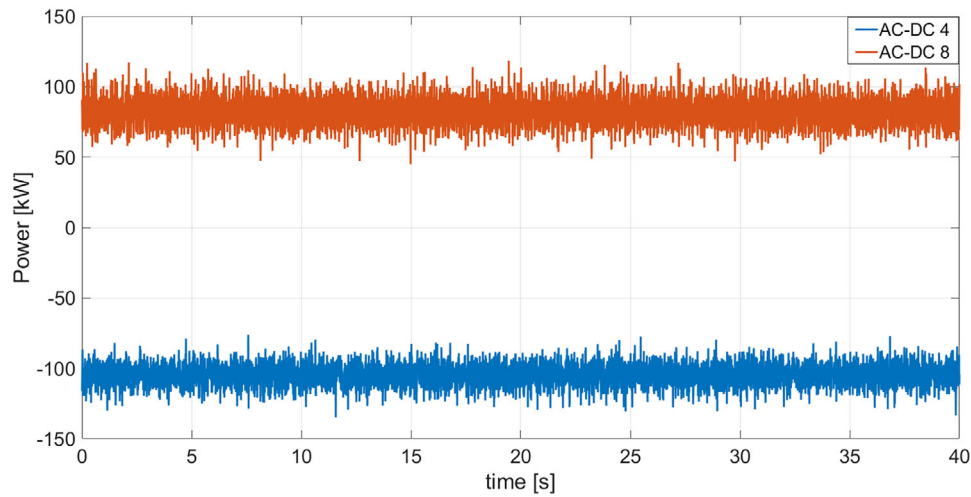


FIGURE 16 Power transients of grid and load converters, experimental data show stability of the power flows.

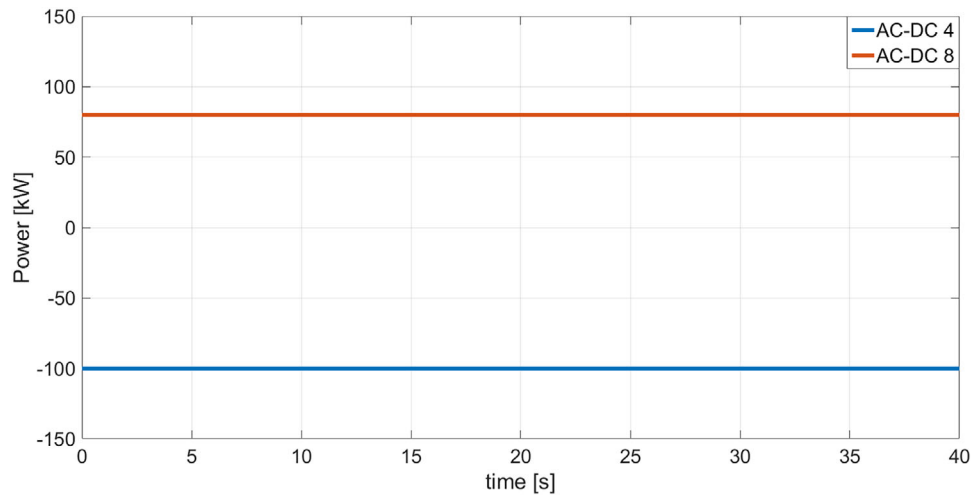


FIGURE 17 Power transients of grid and load converters, C-HIL implementation on RTAI.

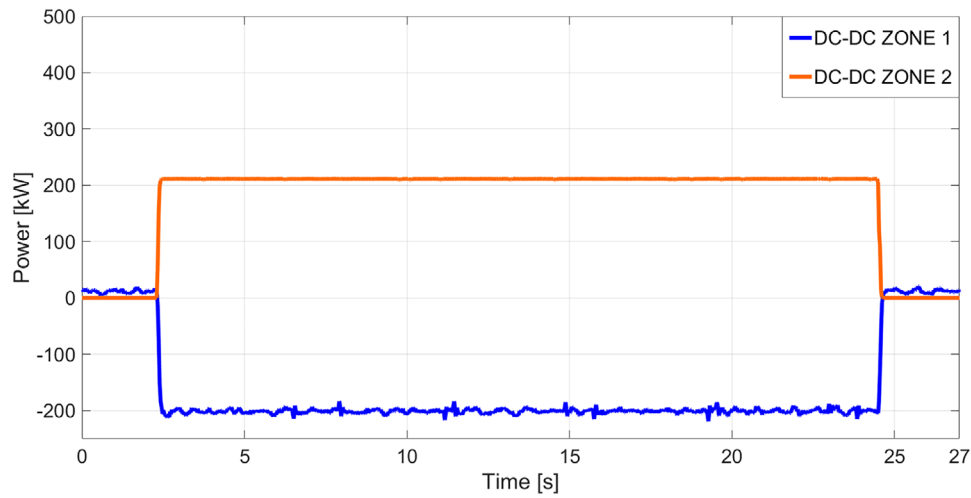


FIGURE 18 Power transients of Zone 1 and Zone 2 converters, experimental data.

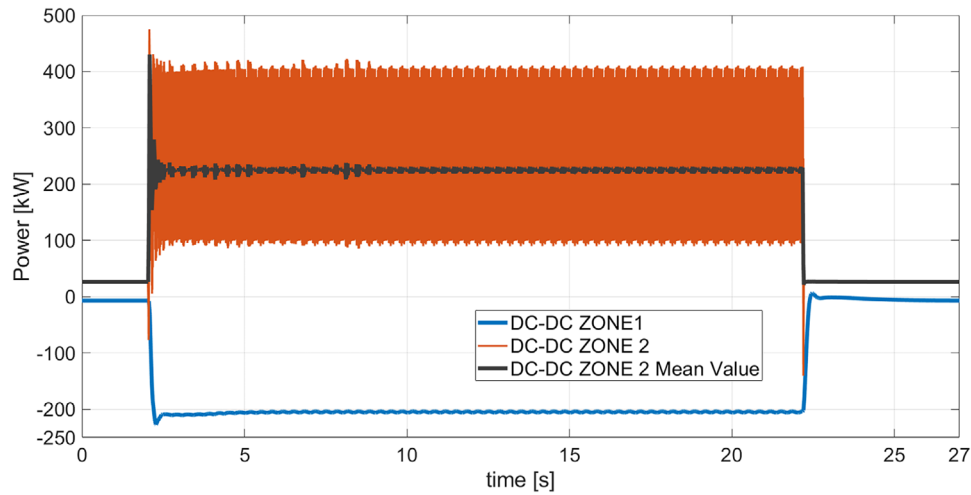


FIGURE 19 Power transients of Zone 1 and Zone 2 converters, C code implementation.

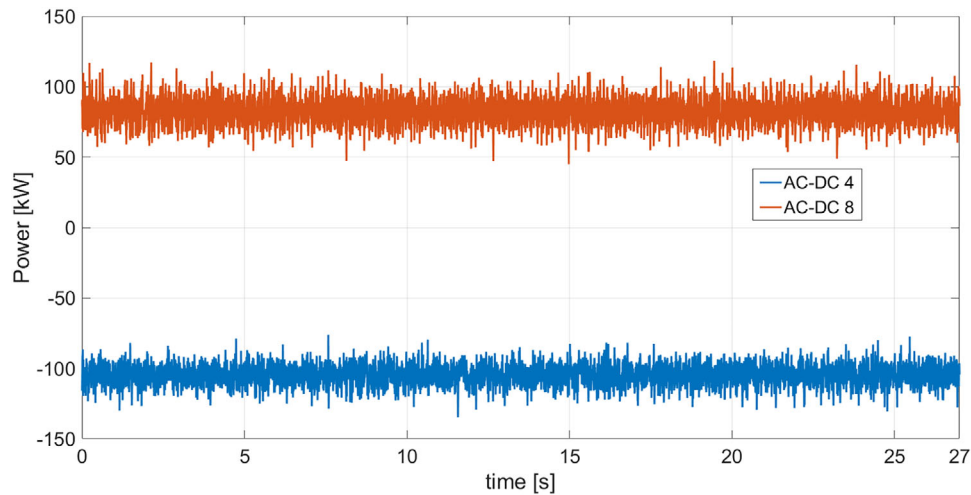


FIGURE 20 Power transients of AC-DC interfacing converters, experimental data.

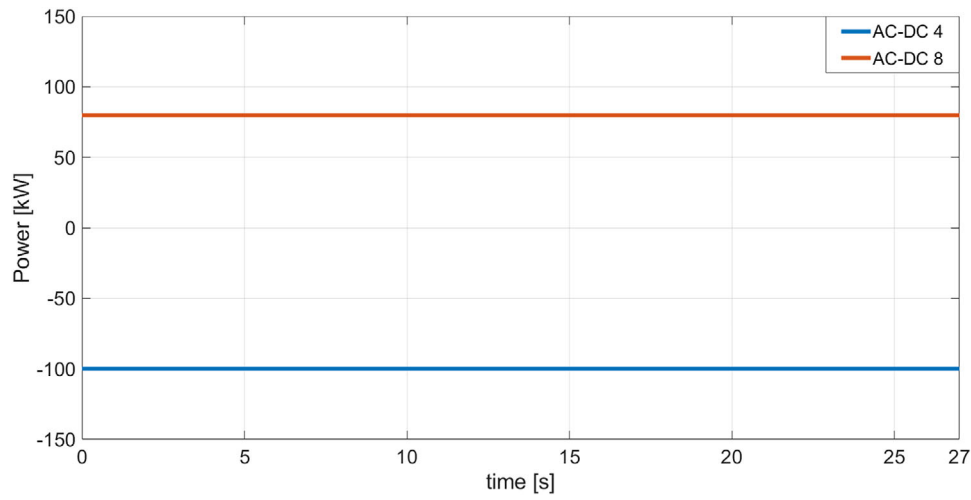


FIGURE 21 Power transients of AC-DC interfacing converters, C code implementation.

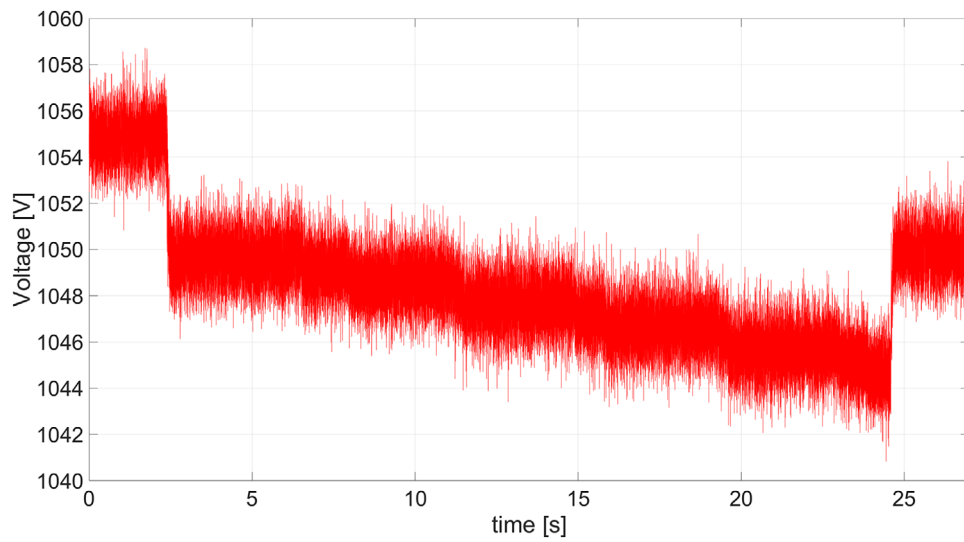


FIGURE 22 Bus voltage transient, experimental data.

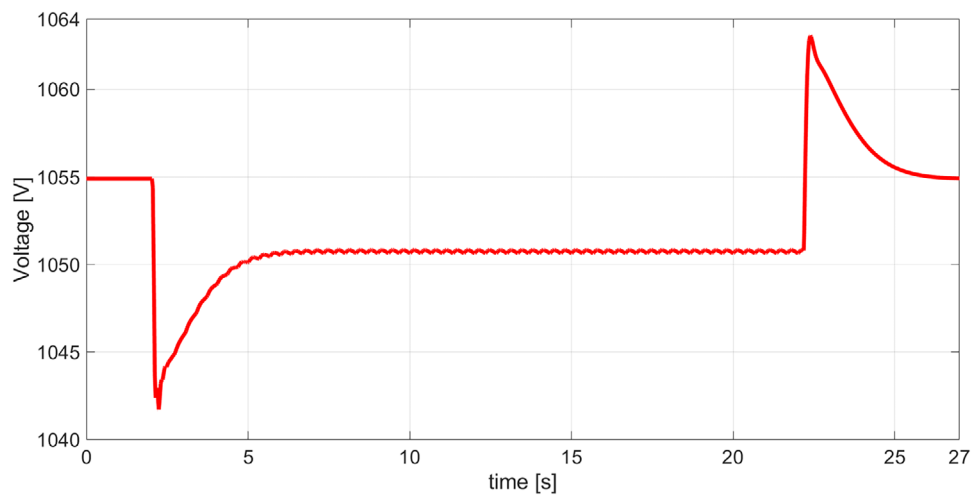


FIGURE 23 Bus voltage transient, C code implantation.

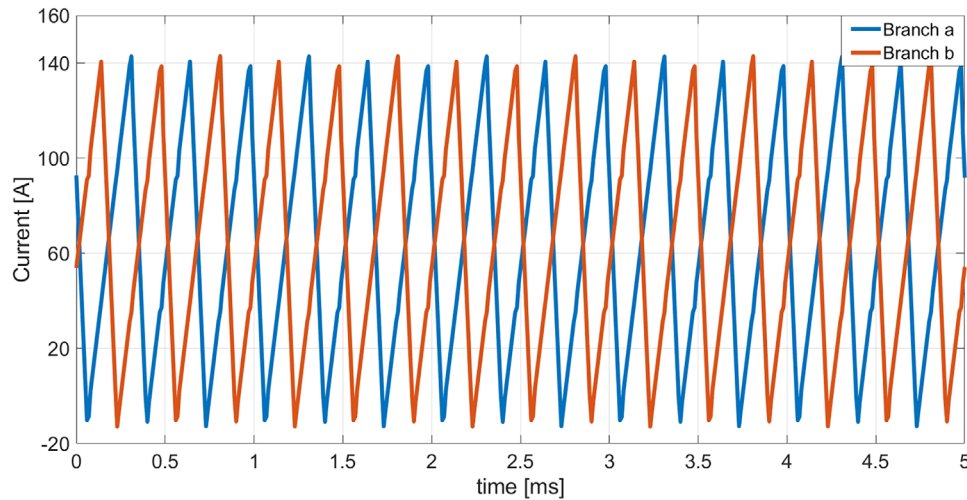


FIGURE 24 Magnification on the current profile for a single DC–DC Zone 2 converter, C code implementation.

8 is requiring approximately 100 kW. This is visible in both the experimental data (Figure 20) and the C-code power transients (Figure 21). During these first seconds, the extra power provided by AC–DC 4 is used to charge the Zone 1 batteries, as shown in both Figures 18 and 19. Since the batteries' converters, DC–DC Zone 1, are regulating the DC bus voltage with an equal droop factor, each perturbation is instantaneously absorbed by the batteries. This is exactly what happens when the Zone 2 electronic load is connected at approximately 2.5 s. At this point, a load step of 200 kW is required by the DC–DC Zone 2 converters and is maintained for approximately 20 s, after which the electronic load is disconnected. This perturbation is shown with an orange line in the power transients of Figures 18 and 19. While the power measurement of the experimental data is highly filtered, in Figure 19 the actual switching behaviour of the converters is visible. This is possible because, while the rest of the system is modelled with AVMs, the Zone 2 components are implemented in Typhoon with the more realistic switching models. However, to better understand the DC–DC Zone 2 converters transients, the mean value of the power is also shown in Figure 19 with a black line. During the 20 s in which the electronic load is connected, the batteries are supplying the Zone 2 load (blue transients of Figures 18 and 19), while the power of the AC–DC converters remains unchanged (Figures 20 and 21). Finally, in Figures 22 and 23 the bus voltage transients of the experimental data and C-code implementation ones are compared. While the initial voltage value is the same for both, during the connection and disconnection of the Zone 2 load the values are different. This is because the droop coefficient is regulated differently in the two implementations. Indeed, the PMS of the real power plant is equipped with an algorithm that modifies the bus voltage reference based on the batteries' SOCs, while the C-code implementation is not yet connected to this real PMS but is controlled in a much simpler-yet-effective manner through the Typhoon SCADA.

The advantage of this C-code implementation is that it makes it possible to model the converters with a higher level of detail compared to the simpler AVM. However, a section of the power

system can still be implemented with AVM, while the portion of interest can be implemented with more detailed switching models. This allows for the observation of the actual current and voltage values at the converter output, as shown in Figures 24 and 25. The DC–DC converters of the power system under study are all two-phase interleaved converters, and in Figure 24 it is possible to see the current on the two branches of one of the DC–DC Zone 2 converters. Finally, in Figure 25, the voltage profile on the DC load of Zone 2 is shown, where the actual voltage ripple is visible. The results of the C-code implementation show the capabilities of the AVM and switching model to work together to achieve the maximum benefits from both modelling approaches in a single simulation setup. While the majority of the power system is simulated using AVMs (that have been proven to represent sufficiently well the behaviour of the power system already in the RTAI implementation), the portion that is modelled in detail with the switching model approach can give more detailed information on the critical parts of the power system.

4.3 | Remarks on the two digital twin implementations

The two digital twin implementations yield satisfactory results, being indeed sufficiently close to the experimental ones. However, some discrepancies can be noted. In particular, while the experimental test and the RTAI implementation share the same PLC controller, the C-code implementation is controlled by a simplified version. This means that the set points can be slightly different, and what is especially evident is that the bus voltage setpoints change during the transients of the experimental and RTAI tests, while these setpoints remain constant for the C-code implementation. This is because the real PLC (demonstrator PMS) includes an algorithm that adjusts the bus voltage setpoint based on the batteries' SOCs. This control logic has yet been integrated into the simplified version of the controller in the C-code implementation; the next step should indeed be to

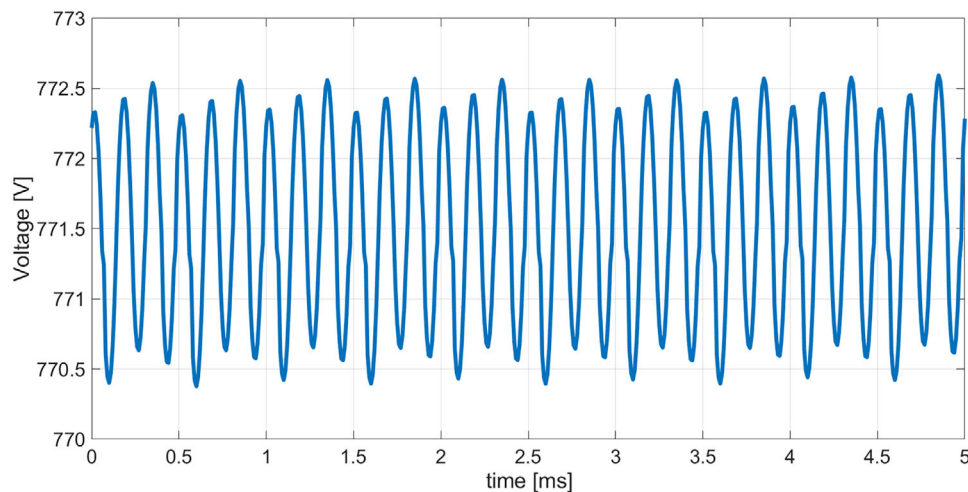


FIGURE 25 Magnification of the voltage profile on a DC load, C code implementation.

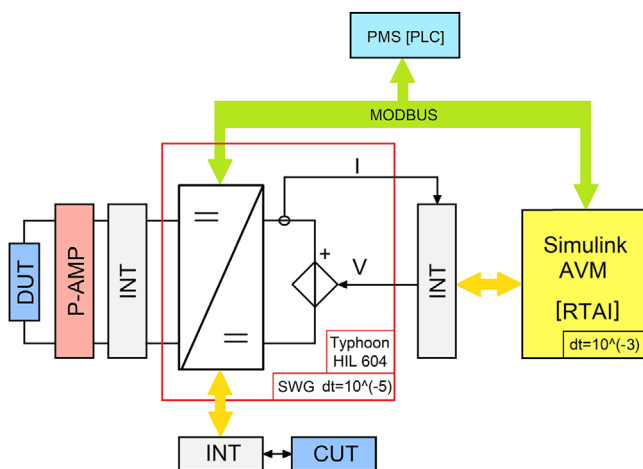


FIGURE 26 RTAI implementation for the P-HIL setup.

connect this setup with the actual PLC. The RTAI implementation allows for a faithful reconstruction of the communication between the PMS and the individual converters. It is also possible to easily include the control logic of each converter in the model by modelling it as a finite state machine. However, simulating the switching of the converter transistors is not feasible. With the current C-code implementation in Typhoon HIL, however, it is possible to simulate the converter up to the transistor switching, but the communication network and the converter logic are not yet integrated.

The C-code Digital Twin implementation, provided in addition to the previously demonstrated RTAI Digital Twin one [30], has been deemed necessary as a required step for the transition from a C-HIL configuration to a P-HIL one. In fact, it provides an interface for future device under tests that is closer to the real-world implementation, thanks to its capability to emulate switching behaviour. The initial idea was to build the Figure 26 setup, in which a portion of the power system is simulated in real-time within the RTAI environment, while the power electronics interface portion is simulated in the Typhoon

environment. Such implementation presents a significant limitation due to the need of interfacing them through a suitable data interface. Indeed, while the Typhoon HIL model runs with a $10 \mu\text{s}$ time step, both RTAI implemented model and communication task are performed with a much slower time step of 1 ms. With such a limitation, no synchronization between the two models was possible at a time step suitable for performing the required simulations. This is the motivation that led to developing and testing the Figure 7 implementation. To complete the discussion, it is proper to observe that the models implemented with RTAI are AVM ones. Therefore, they neglect the switching behaviour of the converters. This reduces the accuracy of the results by neglecting certain converters behaviour, at the same time providing as notable advantages a reduction in the capital cost (and therefore the possibility of implementing similar solutions also with limited capital resources) and the possibility to use commonly available resources for their implementation (i.e. standard PC's). Moreover, it allows to focus on different targets in respect to platforms dedicated to emulating switching behaviour. As an example, it allows a faithful reconstruction of the communication channels between devices (e.g. for testing cybersecurity features), while keeping low the complexity and the computational cost of the non-critical sections of the system.

5 | CONCLUSIONS

Nowadays, resilience is a crucial attribute to be pursued in advanced shipboard microgrids. New solutions based on DC technology can bridge the technological gap to achieve this goal. When the DC power infrastructure is zonal, the distributed presence of autonomously controlled converters enables both smart power usage and enhanced resilience. The widespread adoption of bidirectionally controlled devices ensures effective power routing among generating units, storage systems, and loads. Furthermore, power systems based on DC zonal distribution systems are effective in applying the optimizing algorithms

for the green, safe, and high-performing ship operations. In these microgrids, the real-time cooperation among controlled power electronics converters, facilitated by well-defined communication protocols, is essential for the ship's mission success. To this aim, functional tests are to be done on such shipboard complex power infrastructure. Digital twin approach, as a further step after model-based design, provides the required de-risking step before the onboard placement for controlled systems and related communication. Following this trend, in this paper two HIL implementations of a DC-based power electronics power distribution system have been presented, aiming at realizing a digital twin for a zonal dc shipboard microgrid. The first implementation has been based on an open-source RTOS, while the second has been built upon the Typhoon HIL hardware and software packages. Both the implementations include the mathematical model of the electrical grid and the data network part of the system, although being different in approach and expected performance. Concerning the data network part, the implementation built with RTAI provides greater control over the communication network setting (e.g. individual IP address and protocol implementation can be freely adjusted), but lacks the capability of simulating fast transients like power electronics' switching. Conversely, the implementation built upon Typhoon HIL package forces the use of preset protocols and cards (thus being faster to implement, but less flexible for communication layer testing) but enables the simulation of faster dynamics. Regarding the electrical grid modelling, RTAI implementation requires to build the system's model in Matlab Simulink, which requires some knowledge about power converters modelling through mathematical equations, and requires to prepare specific software links for the data exchange between the model and the real-world. Typhoon HIL instead relies on circuital models and pre-set data links that are easier to manage also for practical engineers, although lacking the flexibility of the former. The selected real-time approach based on the interactions between Typhoon HIL emulation and RTAI simulation (i.e. 100× is the time step ratio to avoid a destabilizing co-presence) is able correctly reproduce both fast and slow dynamics on a zonal DC grid with several controlled power converters. Both solutions demonstrated their capability in correctly emulating the system performance, when compared with experimental results. Therefore, it can be stated that both can be used as a tool for control systems and communication infrastructure de-risking for new DC zonal power systems. Specifically, the RTAI implementation provides greater control on what needs to be simulated and what can instead be modelled with a simplified approach, as well as allowing a finer testing of the communication infrastructure. Its main drawback is the limit on the minimum sampling time for the model, due to the use of general-purpose hardware and software. On the other hand, Typhoon HIL implementation allows the simulation of very fast transients and phenomena thanks to its dedicated hardware and software package, but requires to work directly on its dedicated platform and provides less flexibility in terms of available models and communication interfaces settings.

All in all, it can be stated that tools for performing functional tests on shipboard complex power infrastructures are nowa-

days available. The digital twin approach, as a further step after model-based design, enables to perform the required de-risking step before the onboard placement for controlled systems and related communication. However, the extreme performance required for building a single model capable of performing all the digital twin tasks at all the different layers force towards a new emulation paradigm based on multi-tools methodology. The selection of the correct tool for each de-risking step is critical, and should be made with full awareness of all the available modelling and HIL testing platforms. The best solution may be not relying on a single tool, but building a range of different models, each tailored for a specific need.

AUTHOR CONTRIBUTIONS

Andrea Alessia Tavagnutti: Conceptualization (lead); writing—original draft (lead). **Andrea Vicenzutti:** Formal analysis (lead); writing—review and editing (equal). **Massimiliano Chiandone:** Software (lead); writing—review and editing (equal). **Daniele Bosich:** Methodology (lead); writing—review and editing (equal). **Giorgio Sulligoi:** Conceptualization (supporting); writing—original draft (supporting).

ACKNOWLEDGEMENTS

The authors would like to thank Typhoon HIL for providing the platform used in the development of this research work. Funded by the European Union, Horizon Europe Program—V-ACCESS Project; Grant agreement ID: 101096831. “Views and opinions expressed are however those of the authors only and do not necessarily reflect those of the European Union. Neither the European Union nor the granting authority can be held responsible for them”.

CONFLICT OF INTEREST STATEMENT

The authors declare no conflicts of interest.

DATA AVAILABILITY STATEMENT

Research data are not shared.

ORCID

Daniele Bosich  <https://orcid.org/0000-0001-6475-0079>

REFERENCES

- Siddaiah, R., et al.: Virtual prototyping process: enabling shipboard sizing and arrangement of a power electronics power distribution system. In: 2023 IEEE Electric Ship Technologies Symposium (ESTS), pp. 19–28. IEEE, Piscataway, NJ (2023)
- Blaabjerg, F., Chen, Z., Kjaer, S.B.: Power electronics as efficient interface in dispersed power generation systems. *IEEE Trans. Power Electron.* 19(5), 1184–1194 (2004)
- Ericson, T., Hingorani, N., Khersonsky, Y.: Power electronics and future marine electrical systems. *IEEE Trans. Ind. Appl.* 42(1), 155–163 (2006)
- Vicenzutti, A., Sulligoi, G.: Electrical and energy systems integration for maritime environment-friendly transportation. *Energies* 14, 7240 (2021)
- Kim, S., Kucka, J., Ulissi, G., Kim, S.-N., Dujic, D.: Solid-state technologies for flexible and efficient marine DC microgrids. *IEEE Trans. Smart Grid* 12(4), 2860–2868 (2021)
- Wang, J., Sun, K., Xue, C., Liu, T., Li, Y.: Multi-port DC-AC converter with differential power processing DC-DC converter and flexible power control for battery ESS integrated PV systems. *IEEE Trans. Ind. Electron.* 69(5), 4879–4889 (2022)

7. He, L., et al.: A flexible power control strategy for hybrid AC/DC zones of shipboard power system with distributed energy storages. *IEEE Trans. Ind. Inf.* 14(12), 5496–5508 (2018)
8. IEEE standard for power electronics open system interfaces in zonal electrical distribution systems rated above 100 kW. In: *IEEE Std 1826–2020* (Revision of IEEE Std 1826–2012), pp. 1–44. IEEE, Piscataway, NJ (2020)
9. Petry, C.R., Rumburg, J.W.: Zonal electrical distribution systems: an affordable architecture for the future. *Nav. Eng. J.* 105, 45–51 (1993)
10. Wasynczuk, O., Walters, E.A., Hegner, H.J.: Simulation of a zonal electric distribution system for shipboard applications. In: *IECEC-97 Proceedings of the Thirty-Second Intersociety Energy Conversion Engineering Conference*, vol. 1, pp. 268–273. IEEE, Piscataway, NJ (1997)
11. Ciezki, J.G., Ashton, R.W.: The application of a customized DSP board for the control of power electronic converters in a DC zonal electric distribution system. In: *Conference Record of Thirty-Second Asilomar Conference on Signals, Systems and Computers*, vol. 2, pp. 1017–1021. IEEE, Piscataway, NJ (1998)
12. IEEE recommended practice for the design and application of power electronics in electrical power systems. In: *IEEE Std 1662–2016* (Revision of IEEE Std 1662–2008), pp. 1–68. IEEE, Piscataway, NJ (2017)
13. IEEE guide for control architecture for high power electronics (1 MW and greater) used in electric power transmission and distribution systems. In: *IEEE Std 1676–2010*, pp. 1–47. IEEE, Piscataway, NJ (2011)
14. Sulligoi, G., Bosich, D., Vicenzutti, A., Khersonsky, Y.: Design of zonal electrical distribution systems for ships and oil platforms: control systems and protections. *IEEE Trans. Ind. Appl.* 56(5), 5656–5669 (2020)
15. Khersonsky, Y., Hingorani, N., Peterson, K.L.: IEEE electric ship technologies initiative. *IEEE Ind. Appl. Mag.* 17(1), 65–73 (2011)
16. Doerry, N., McCoy, K.: Next generation integrated power system, ngips technology development roadmap. Naval Sea Systems Command (2007)
17. NPES technology development roadmap. Naval Sea Systems Command (2019)
18. Ma, Y., Corzine, K., Maqsood, A., Gao, F., Wang, K.: Stability assessment of droop controlled parallel buck converters in zonal ship DC microgrid. In: *Proceedings of the 2019 IEEE Electric Ship Technologies Symposium (ESTS)*, pp. 268–272. IEEE, Piscataway, NJ (2019)
19. Sulligoi, G., Bosich, D., Giadrossi, G., Zhu, L., Cupelli, M., Monti, A.: Multiconverter medium voltage dc power systems on ships: constant-power loads instability solution using linearization via state feedback control. *IEEE Trans. Smart Grid* 5(5), 2543–2552 (2014)
20. Maqsood, A., Corzine, K.A.: Integration of Z-source breakers into zonal DC ship power system microgrids. *IEEE J. Emerging Sel. Top. Power Electron.* 5(1), 269–277 (2017)
21. Christopher, E., Sumner, M., Thomas, D.W.P., Wang, X., Wildt, F.D.: Fault location in a zonal DC marine power system using active impedance estimation. *IEEE Trans. Ind. Appl.* 49(2), 860–865 (2013)
22. Perkins, D., Vu, T., Vahedi, H., Edrington, C.S.: Distributed power management implementation for zonal MVDC ship power systems. In: *Proceedings of IECON 2018 - 44th Annual Conference of the IEEE Industrial Electronics Society*, pp. 3401–3406. IEEE, Piscataway, NJ (2018)
23. Mariam, L., Basu, M., Conlon, M.F.: A review of existing microgrid architectures. *J. Eng.* 2013, 937614 (2013)
24. Suryanarayanan, S., Steurer, M., Woodruff, S., Meeker, R.: Research perspectives on high-fidelity modeling, simulation and hardware-in-the-loop for electric grid infrastructure hardening. In: *2007 IEEE Power Engineering Society General Meeting*, pp. 1–4. IEEE, Piscataway, NJ (2007)
25. Channegowda, J., Saritha, B., Chola, H.R., Narayanan, G.: Comparative evaluation of switching and average models of a DC-DC boost converter for real-time simulation. In: *2014 IEEE International Conference on Electronics, Computing and Communication Technologies (CONECCT)*, pp. 1–6. IEEE, Piscataway, NJ (2014)
26. Meng, X., et al.: Combining detailed equivalent model with switching-function-based average value model for fast and accurate simulation of MMCs. *IEEE Trans. Energy Convers.* 35(1), 484–496 (2020)
27. Kuanar, A., Panda, B., Behera, D.: Comparison of simulation tools for load flow analysis. In: *2021 1st International Conference on Power Electronics and Energy (ICPEE)*, pp. 1–5. IEEE, Piscataway, NJ (2021)
28. Tu, H., Du, Y., Yu, H., Dubey, A., Lukic, S., Karsai, G.: Resilient information architecture platform for the smart grid: a novel open-source platform for microgrid control. *IEEE Trans. Ind. Electron.* 67(11), 9393–9404 (2020)
29. Quaranta, G., Mantegazza, P.: *Using MATLAB-simulink RTW to build real time control applications in user space with RTAI-LXRT. Realtime Linux: Workshop*, Milano (2001)
30. Bosich, D., Chiandone, M., Sulligoi, G., Tavagnutti, A.A., Vicenzutti, A.: High-performance megawatt-scale MVDC zonal electrical distribution system based on power electronics open system interfaces. *IEEE Trans. Transp. Electrification* 9(3), 4541–4551 (2023)
31. IEEE recommended practice for 1 kV to 35 kV medium-voltage DC power systems on ships. In: *IEEE Std 1709–2018* (Revision of IEEE Std 1709–2010), pp. 1–54. IEEE, Piscataway, NJ (2018)
32. Vicenzutti, A., Sulligoi, G.: Protections in a MW-scale DC ZEDS based on COTS components. In: *2021 IEEE Fourth International Conference on DC Microgrids (ICDCM)*, pp. 1–8. IEEE, Piscataway, NJ (2021)
33. Ericson, T., Khersonsky, Y., Schugart, P., Steimer, P.: PEBB—power electronics building blocks, from concept to reality. In: *2006 3rd IET International Conference on Power Electronics, Machines and Drives—PEMD 2006*, pp. 12–16. IET, London (2006)
34. Chiandone, M., Vicenzutti, A., Bosich, D., Tavagnutti, A.A., Barbini, N., Sulligoi, G.: Open source hardware in the loop real-time simulation of zonal DC systems. In: *Proceedings of the 2022 Open Source Modelling and Simulation of Energy Systems (OSMES)*, pp. 1–6. IEEE, Piscataway, NJ (2022)
35. Zhang, W., Wang, L., Wang, L., Liao, C., Zhang, Y.: Joint state-of-charge and state-of-available-power estimation based on the online parameter identification of lithium-ion battery model. *IEEE Trans. Ind. Electron.* 69(4), 3677–3688 (2022)
36. Campagna, N.; Castiglia, V.; Miceli, R.; Mastromauro, R.A.; Spataro, C.; Trapanese, M.; Viola, F.: Battery models for battery powered applications: a comparative study. *Energies* 13, 4085 (2020)
37. Tremblay, O., Dessaint, L.-A., Dekkiche, A.-I.: A Generic battery model for the dynamic simulation of hybrid electric vehicles. In: *2007 IEEE Vehicle Power and Propulsion Conference*, pp. 284–289. IEEE, Piscataway, NJ (2007)
38. Tavagnutti, A.A., Bosich, D., Sulligoi, G.: A multi-model methodology for stability assessment of complex DC microgrids. In: *Proceedings of the 2021 IEEE Fourth International Conference on DC Microgrids (ICDCM)*, pp. 1–7. IEEE, Piscataway, NJ (2021)
39. Hou, C.-C., Cheng, P.-T.: Experimental verification of the active front-end converters dynamic model and control designs. *IEEE Trans. Power Electron.* 26(4), 1112–1118 (2011)
40. Jin, Z., Meng, L., Guerrero, J.M., Han, R.: Hierarchical control design for a shipboard power system with DC distribution and energy storage aboard future more-electric ships. *IEEE Trans. Ind. Inf.* 14(2), 703–714 (2018)
41. Dragičević, T., Lu, X., Vasquez, J.C., Guerrero, J.M.: DC microgrids—part I: a review of control strategies and stabilization techniques. *IEEE Trans. Power Electron.* 31(7), 4876–4891 (2016)
42. Nguyen, T.L., Guerrero, J.M., Griepentrog, G.: A self-sustained and flexible control strategy for islanded DC nanogrids without communication links. *IEEE J. Emerging Sel. Top. Power Electron.* 8(1), 877–892 (2020)
43. Lu, X., Sun, K., Guerrero, J.M., Vasquez, J.C., Huang, L.: State-of-charge balance using adaptive droop control for distributed energy storage systems in DC microgrid applications. *IEEE Trans. Ind. Electron.* 61(6), 2804–2815 (2014)
44. Sulligoi, G., Chiandone, M., Arcidiacono, V.: NewSART automatic voltage and reactive power regulator for secondary voltage regulation: design and application. In: *2011 IEEE Power and Energy Society General Meeting*, pp. 1–7. IEEE, Piscataway, NJ (2011)
45. Jiang, F., Gao, S., Zhang, J.: A hardware-in-the-loop simulation system of diesel engine based on Linux RTAI. In: *2009 Asia-Pacific Power and Energy Engineering Conference*, pp. 1–4. IEEE, Piscataway, NJ (2009)
46. Lou, L., Kühnlenz, K.: Hardware-in-the-loop development and real-time testing for precision motion control under RTAI. In: *2014 13th International Conference on Control Automation Robotics & Vision (ICARCV)*, pp. 312–316. IEEE, Piscataway, NJ (2014)

47. Chiandone, M., Sulligoi, G.: Performance assessment of a motion control application based on Linux RTAI. In: Proceedings of SPEEDAM 2010, pp. 687–692. IEEE, Piscataway, NJ (2010)
48. Barbalace, A., Luchetta, A., Manduchi, G., Moro, M., Soppelsa, A., Taliercio, C.: Performance comparison of VxWorks, Linux, RTAI, and Xenomai in a hard real-time application. *IEEE Trans. Nucl. Sci.* 55(1), 435–439 (2008)
49. Libmodbus library. <https://libmodbus.org/>
50. Chiandone, M., Merola, M., Vicenzutti, A., Sulligoi, G., Marcelli, G.M.: A holistic approach for the dependability enforcement of cyber & power systems on future MVDC ships. *NMIOTC Marit. Interdiction Oper. J.* 24, 41–49 (2022)

How to cite this article: Tavagnutti, A.A., Vicenzutti, A., Chiandone, M., Bosich, D., Sulligoi, G.: The digital twin of complex shipboard DC microgrids: the high-performing synergy of compiled models and HIL platform in the dynamics emulation of zonal power electronic power distribution systems. *IET Power Electron.* 18, e12835 (2025).

<https://doi.org/10.1049/pel2.12835>